Transient Activations of Rac1 at the Lamellipodium Tip Trigger Membrane Protrusion

Amine Mehidi, Olivier Rossier, Matthias Schaks, Anaël Chazeau, Fabien Biname, Amanda Remorino, Mathieu Coppey, Zeynep Karatas, Jean-Baptiste Sibarita, Klemens Rottner, et al.

Version of Record: https://www.sciencedirect.com/science/article/pii/S0960982219308802
Manuscript_28c5fff2863c7461aa2bad6ca246a135

Transient activations of Rac1 at the lamellipodium tip trigger membrane protrusion

Amine Mehidi[1,2], Olivier Rossier[1,2], Matthias Schaks[3,4], Anaël Chazeau[1,2,5], Fabien Binamé[6], Amanda Remorino[7], Mathieu Coppey[7], Zeynep Karatas[1,2], Jean-Baptiste Sibarita[1,2], Klemens Rottner[3,4], Violaine Moreau[6], Grégory Giannone[1,2*]

[1]Univ. Bordeaux, Interdisciplinary Institute for Neuroscience, UMR 5297, F-33000 Bordeaux, France
[2]CNRS, Interdisciplinary Institute for Neuroscience, UMR 5297, F-33000 Bordeaux, France
[3]Division of Molecular Cell Biology, Zoological Institute, Technische Universität Braunschweig, Spielmannstrasse 7, 38106 Braunschweig
[4]Department of Cell Biology, Helmholtz Centre for Infection Research, Inhoffenstrasse 7, 38124 Braunschweig
[5]Present address: Cell Biology, Faculty of Science, Utrecht University, Padulaan 8 3584 CH Utrecht, the Netherlands;
[6]INSERM, Université de Bordeaux, UMR1053 Bordeaux Research In Translational Oncology, BaRITOn, F-33000 Bordeaux, France.
[7]Laboratoire Physico-Chimie, Institut Curie, CNRS UMR168, Paris-Science Lettres, Universite Pierre et Marie Curie-Paris 6, 75005 Paris, France.

*Authors for correspondence: Grégory Giannone
Lead contact: Grégory Giannone, Email: gregory.giannone@u-bordeaux.fr

Condensed title: Fast Rac1 activation cycles at the lamellipodium tip

Summary

The spatiotemporal coordination of actin regulators in the lamellipodium determines the dynamics and architecture of branched F-actin networks during cell migration. The WAVE regulatory complex (WRC), an effector of Rac1 during cell protrusion, is concentrated at the lamellipodium tip. Thus, activated Rac1 should operate at this location to activate WRC and trigger membrane protrusion. Yet, correlation of Rho GTPase activation with cycles of membrane protrusion previously revealed complex spatiotemporal patterns of Rac1 and RhoA activation in the lamellipodium. Combining single protein tracking (SPT) and super-resolution imaging with loss- or gain-of-function mutants of Rho GTPases, we show that Rac1 immobilizations at the lamellipodium tip correlate with its activation, in contrast to RhoA. Using Rac1 effector loop mutants and wild-type *versus* mutant variants of WRC, we show that selective immobilizations of activated Rac1 at the lamellipodium tip depend on effector binding, including WRC. In contrast, wild-type Rac1 only displays slower diffusion at the lamellipodium tip, suggesting transient activations. Local optogenetic activation of Rac1, triggered by membrane recruitment of Tiam1, shows that Rac1 activation must occur close to the lamellipodium tip and not behind the lamellipodium to trigger efficient membrane protrusion. However, coupling tracking with optogenetic activation of Rac1 demonstrates that diffusive properties of wild type Rac1 are unchanged despite enhanced lamellipodium protrusion. Taken together, our results support a model whereby transient activations of Rac1 occurring close to the lamellipodium tip trigger WRC binding. This short-lived activation ensures a local and rapid control of Rac1 actions on its effectors to trigger actin-based protrusion.

Key Words: Cell migration / lamellipodium / branched F-actin regulators / Rho GTPases / single protein tracking / super-resolution microscopy

Introduction

Cell motility is critical for physiological phenomena like embryogenesis, immunological responses, wound healing and growth cone pathfinding. Deregulation of cell motility contributes to pathologies including cancer cell dissemination [1]. The first step in motility is the protrusion of a lamellipodium, a thin sheet of membrane-enclosed F-actin networks propelled by actin polymerization [2,3]. Rho GTPases are molecular switches controlling cytoskeletal rearrangements during cell growth, adhesion, and motility [4]. Among them, Rac1 activation is the major signal driving lamellipodium formation [5–7]. Rac1 is targeted to the plasma membrane where it can bind and activate the WAVE regulatory complex (WRC), a nucleation promoting factor stimulating the Arp2/3 complex and thus branched F-actin nucleation [8,9]. Filament length is controlled by elongation factors including VASP, Formin-Like protein 2 (FMNL2) [10,11] and heterodimeric capping protein [12]. Finally, F-actin turnover is driven by severing proteins such as ADF/cofilin [13] or myosin motors [14]. The actions of actin regulators in the lamellipodium are highly compartmentalized [13,15]. Actin nucleation, branching, and elongation occur at the lamellipodium tip [2], whereas myosin II generates forces at the lamellipodium rear [16], and ADF/cofilin ensures F-actin severing throughout the lamellipodium [13]. From the complex spatiotemporal coordination of actin regulators at the nanometer scale could emerge the micron-scale periodic phenomenon driving lamellipodium protrusion [16–18].

The development of super-resolution microscopy techniques [19,20] and single protein tracking (SPT) [21,22] has revolutionized biomolecular imaging in cells. Super-resolution microscopy studies previously explored sub-cellular structures including integrin-based adhesions [23,24], neuronal axons [25] and dendritic spines [26]. Those studies unraveled that proteins seemingly co-localized with conventional light microscopy are spatially segregated into distinct functional domains at the nanoscale level. The lamellipodium is also a polarized structure organized into functional domains, the tip, the core, and the rear. The localization of most actin-binding proteins and regulators in the lamellipodium, obtained using conventional fluorescent microscopy, are in good agreement with their functions [13,15,16,27]. Nevertheless, sites of action of signaling proteins are often difficult to localize. Rac1 is associated with lamellipodium formation since more than a decade [5–7]. Because WRC accumulates at the lamellipodium tip [13,28], activated Rac1 should reside at this location to stimulate WRC activation. However, FRET-based experiments, which correlated Rac1 and RhoA activities with membrane protrusion cycles, reported that the peak of Rac1 activation is not synchronized with the onset of membrane protrusion, and occurs 2 μm away from the lamellipodium tip [29]. In contrast, the peak of RhoA activation is located at the cell edge [30] and synchronized with edge progression [29]. Consequently, sites of Rac1 activation might be distinct from sites of Rac1-mediated WRC activation. However, the spatial resolution of conventional fluorescent microscopy is in specific instances insufficient to fully decrypt the sequence of molecular events controlling actin network dynamics within protrusive structures. In this study, we used SPT and super-resolution microscopy, to obtain molecular resolution of the dynamics and localizations of Rac1 and RhoA inside and outside the lamellipodium. Combining these techniques with loss- or gain-of-function of Rho GTPase mutants, we linked the nanoscale organization and dynamics of Rac1 to its activation and site of action within the lamellipodium. In addition, we used optogenetics to trigger spatially-controlled Rac1 activations and study their consequences on Rac1 molecular dynamics and membrane protrusion.

Results

WRC and IRSp53 are recruited to the lamellipodium tip by membrane free-diffusion.

Nucleation of F-actin branches requires the coordination in space and time of different signals involving GTP-bound Rac1, the WAVE regulatory and Arp2/3 complexes, IRSp53 and acidic phospholipids (PIP3) [8,9,31–33]. To determine the sequence of molecular events leading to Rac1-dependent WRC activation, we performed high-frequency sptPALM acquisition (50 Hz) to characterize the diffusive properties of actin regulators in the lamellipodium [24,34]. Mouse embryonic fibroblasts (MEFs) were co-transfected with mEos2-fused proteins and α-actinin-GFP, as a lamellipodium reporter, and seeded onto fibronectin-coated coverslips. To limit experimental variability, we performed acquisitions on cells displaying isotropic spreading, which is powered by lamellipodia devoid of filopodia or mature focal adhesions [16,17]. Since Rac1 is also activated by growth factors [5], experiments were performed in serum-free medium to focus on integrin-dependent Rac1 activation [35,36]. SptPALM sequences (30 s) were acquired in between α-actinin-GFP images to visualize lamellipodium displacement (Figure 1, Video S1). We reconstructed and analyzed thousands of mEos2-fused protein trajectories, sorted between the lamellipodium tip and the region outside of the lamellipodium (Figure 1A, see methods). For trajectories lasting more than 260 ms (> 13 points), we computed the mean squared displacement (MSD), which describes the diffusive properties of a molecule. We sorted trajectories according to their diffusion modes (immobile, confined, free-diffusive) and extracted their diffusion coefficients (D) (Figures 1 and S1, Data S1A, Video S1) [24,26,34]. Within the spatial resolution of our experiments (~59 nm), all molecules with a D inferior to 0.011 $\mu m^2.s^{-1}$ are classified as immobile.

To characterize the diffusive behavior of a control protein anchored to the inner leaflet of the plasma membrane, we used mEos2 fused to a CAAX prenylation sequence. mEos2-CAAX displayed a low fraction of immobilization and fast free-diffusion both at the lamellipodium tip (9 ± 2 %; D_{diff} = 0.679 $\mu m^2.\ s^{-1}$) and at the membrane outside the lamellipodium (11 ± 2 %; D_{diff} = 0.721 $\mu m^2.\ s^{-1}$) (Figures 1D and E-G, Data S1A). From sptPALM sequences, we generated single-molecule-based super-resolution intensity images [24,26], showing no selective immobilizations of mEos2-CAAX at the lamellipodium tip (Figure 1D). WRC comprises five subunits: Wave2, Abi1, Nap1, Brick and Sra1 [37,38]. The WRC subunit, mEos2-Abi1, displayed a larger fraction of membrane free-diffusion outside the lamellipodium compared to the lamellipodium tip (tip: 22 ± 2 %; outside: 34 ± 1 %) (1B, E-G, Video S1, Data S1A). Super-resolution intensity images showed selective immobilizations of mEos2-Abi1 at the lamellipodium tip (Figure 1B), corresponding to locations where repetitive mEos2 fluorescence signals were detected, and explained the increased fraction of immobilizations at this location (tip: 58 ± 2 %; outside: 44 ± 2 %)(Figures 1E and F, Video S1). Thus, our results suggest that WRC is recruited to the lamellipodium tip by a diffusion trapping mechanism, in line with a previous study using SPT in *Xenopus* cells [39]. Those selective immobilizations are not mediated by protein crowding or membrane curvature since the diffusive behavior of mEos2-CAAX was identical inside and outside the lamellipodium tip, but probably reflect specific interactions with proteins at the lamellipodium tip. We next examined the behavior of an I-BAR domain protein, IRSp53, which drives negative membrane curvature [40] and has previously been reported to contribute to Rac signaling to WRC [9,41–43]. The diffusive behavior of mEos2-IRSp53 was similar to mEos2-Abi1, exhibiting membrane free-diffusion out of the lamellipodium and selective immobilizations at the

lamellipodium tip (Figures 1C and E-G, Data S1A). Thus, like WRC, IRSp53 is recruited to the lamellipodium tip by a diffusion-trapping mechanism.

Rac1 immobilization at the lamellipodium tip correlates with its activation state.

Many studies demonstrated that WRC is a critical downstream target of Rac1 triggering cell edge protrusion [5–7,44]. To test whether selective immobilizations of WRC were triggered by interactions with Rac1 bound to the lamellipodium tip, we performed sptPALM acquisition on wild-type (WT) Rac1. The molecular dynamics of mEos2-Rac1-WT were largely dominated by membrane free-diffusion at the lamellipodium tip and at the membrane outside the lamellipodium (tip: 59 ± 2 %; outside: 63 ± 1 %) (Figures 2A and E-G, Data S1A). Although the fraction of immobilization was not significantly increased at the lamellipodium tip compared to CAAX-mEos2 (Rac1: 13 ± 1 %; CAAX: 9 ± 2 %) (Figure 2F), the mean coefficient of free-diffusion (D_{diff}) was significantly decreased (Rac1: D_{diff} = 0.519 $\mu m^2.s^{-1}$; CAAX: D_{diff} = 0.679 $\mu m^2.s^{-1}$) (Figure 2G). These results suggest that transient interactions of Rac1 with biomolecules at the lamellipodium tip are slowing down its movements. The large disparity of dynamic behaviors between mEos2-Abi1 and mEos2-Rac1-WT supports the idea that Rac1 is not responsible for the selective immobilization of WRC at the lamellipodium tip.

A correlation between Rac1 activation and its immobilization was demonstrated in adhesive structures, including focal adhesions and dendritic spines [26,45], but also in signaling nanoclusters of polarized cells [46]. To determine whether Rac1 activation state controls its localization and diffusive behavior in the lamellipodium, we performed sptPALM experiments on well-characterized Rac1 mutants (Figures 2B and D). The constitutively active Rac1 mutant (Rac1-Q61L) is locked in its GTP-bound state, which is the conformation binding and activating Rac1 effectors. Strikingly, and in contrast to Rac1-WT, super-resolution intensity images displayed selective immobilizations of mEos2-Rac1-Q61L at the lamellipodium tip (Figure 2B). Distributions of D were shifted towards slower diffusion (Figure 2E), and the fraction of immobilization at the lamellipodium tip was increased (Rac1-Q61L: 31 ± 2 %; Rac1-WT: 13 ± 1 %) (Figure 2F), but did not reach the level of immobilization measured for WRC (58 ± 2 %) (Figure 1F). These results suggest that Rac1-Q61L immobilizations at the lamellipodium tip are transient events and could explain why classical fluorescence microscopy could not reveal enrichment of active Rac1 at the lamellipodium tip [36]. In agreement with increased interactions of Rac1-Q61L with its effectors, D_{diff} were also significantly decreased at the lamellipodium tip compared to Rac1-WT (Rac1-Q61L: D_{diff} = 0.373 $\mu m^2.s^{-1}$; Rac1-WT: D_{diff} = 0.519 $\mu m^2.s^{-1}$) (Figure 2G). The fast cycling mutant Rac1-F28L, which is comparable to the Rac1-P29S mutation found in melanoma [47], switches more frequently to the activated state as a result of an increased GDP to GTP nucleotide exchange. Interestingly, mEos2-Rac1-F28L exhibited a fraction of immobilization and diffusive behavior closer to mEos2-Rac1-WT than to mEos2-Rac1-Q61L (Figures 2D and G). This suggests that Rac1-WT remains in its active state only transiently. We also used an inactive Rac1 mutant (Rac1-T17N), which is nucleotide free, and therefore locked in its inactive conformation unable to bind effectors. Like mEos2-CAAX membrane control, mEos2-Rac1-T17N was dominated by fast free-diffusion and did not display selective immobilizations at the lamellipodium tip or decreased free-diffusion, like WT and active mutants of Rac1 (Figures 2C and E-G, Data S1A). Our results thus show a correlation between Rac1 activation and its selective immobilization at the lamellipodium tip where WRC resides.

Activated Rac1 immobilization at the lamellipodium tip depends on effector binding

Next, we tested whether selective immobilizations of activated Rac1 at the lamellipodium tip are triggered by effector interactions. We performed experiments with Rac1 mutants in the loop domain affecting effector binding, the F37A-mutation of Rac1 impairing lamellipodium formation and p160ROCK binding, and the Y40C-mutation abrogating PAK binding [36,48,49], in combination with the Q61L-mutation triggering Rac1 constitutive activation (Figure 3). The diffusive behavior of mEos2-Rac1-Y40C-Q61L was identical to mEos2-Rac1-Q61L, both at the lamellipodium tip and outside the lamellipodium (Figures 3B and E-G, Data S1A). In contrast, mEos2-Rac1-F37A-Q61L displayed a decreased fraction of immobilization and faster free-diffusion compared to mEos2-Rac1-Q61L and mEos2-Rac1-Y40C-Q61L at the lamellipodium tip (Figures 3D and E-G, Data S1A). These results suggested that the larger fraction of immobilization measured at the lamellipodium tip for activated Rac1-Q61L depends on binding to effectors involved in lamellipodium formation, e.g. WRC.

To characterize the interaction between Rac1-F37A-Q61L and WRC, we immunoprecipitated distinct Rac1 variants in B16 cells in which endogenous Sra1 and PIR121 had been genetically disrupted by CRISPR/Cas9 (Sra1/PIR121-KO) (Figure S2)[44]. Endogenous Sra1/PIR121 had been replaced by mCherry-tagged, wild-type Sra1 (Sra1-WT) or a variant leading to constitutive WRC activation (Sra1-WCA*) by destabilized interactions with W- and C-regions of WAVE. Previous results showed that active WRC (harboring Sra1-WCA*) binds constitutively active EGFP-Rac1-Q61L better than wild-type WRC (harboring Sra1-WT) [8,44]. However, EGFP-tagged Rac1-F37A-Q61L displayed a decreased binding to both wild-type and constitutively active WRC (Figure S2). Consistently, B16 cells genetically depleted for all Rac GTPases (Rac1/2/3) formed morphologically compromised lamellipodia upon expression of EGFP-Rac1-F37A-Q61L as compared to EGFP-Rac1-Q61L [44], as confirmed by quantitation (Figure S2).

Then we performed sptPALM experiments in migrating B16 Sra1/PIR121-KO cells rescued with Sra1-WT (Figures 4A,B and S3, Data S1B). Like in MEFs, distributions of D for mEos2-Rac1-Q61L compared to mEos2-Rac1-WT were shifted towards slower diffusion (Figure 4E), the fraction of immobilization at the lamellipodium tip was increased (Rac1-Q61L: 14 ± 1 %; Rac1-WT: 9 ± 2 %)(Figures 4F and I), and D_{diff} were also decreased at the lamellipodium tip (Rac1-Q61L: D_{diff} = 0.540 $\mu m^2.s^{-1}$; Rac1-WT: D_{diff} = 0.698 $\mu m^2.s^{-1}$) (Figure 4J). This confirmed the correlation between Rac1 activation and its selective immobilization at the lamellipodium tip in B16 cells. Although immobilization fractions were overall reduced in this cell type, our results with this model of lamellipodia-based migration extend our results previously obtained with fibroblasts. In B16 Sra-1/PIR121 KO cells expressing Sra1-WCA*, mEos2-Rac1-Q61L displayed an increase of its immobilization fraction and slower free-diffusion compared to cells expressing Sra1-WT (Figures 4F, I and J). In addition, durations of mEos2-Rac1-Q61L immobilizations at the lamellipodium tip were increased in cells expressing Sra1-WCA* (and thus active WRC) compared to Sra1-WT (Figures 4K-M), leading to a striking accumulation of mEos2-Rac1-Q61L at the lamellipodium tip (Figure 4C). Thus, constitutive WRC activation increases binding to activated Rac1-Q61L [44] and the selective immobilization of Rac1-Q61L at the lamellipodium tip (Figure 4). Importantly, as observed in MEFs, mEos2-Rac1-F37A-Q61L displayed a decreased fraction of immobilization and faster free-diffusion at the lamellipodium tip compared to mEos2-Rac1-Q61L both in the context of Sra1-WT and Sra1-WCA* (Figures 4D, G-J and S3). Thus, the F37A-Rac1 mutation decreases binding to WRC (Figure S2), lamellipodia formation (Figure S2), and selective immobilization of activated Rac1-Q61L at the lamellipodium tip (Figures 3 and 4). Taken

together, our results support the hypothesis that immobilizations of activated Rac1 depends at least partly on binding to WRC.

RhoA does not display selective immobilization at the lamellipodium tip

FRET-based sensors showed that strongest RhoA activation encompassed the lamellipodium tip [30] and that its activation peak was correlated with the onset of lamellipodium protrusion [29]. To investigate if RhoA was selectively immobilized at the lamellipodium tip, we performed sptPALM experiments using mEos2-RhoA-WT. Like Rac1-WT, the dynamic behavior of RhoA-WT was dominated by membrane free-diffusion (tip: 58 ± 4 %; outside: 59 ± 3 %) (Figures 5A and D-F, Data S1A). The fraction of immobilization at the lamellipodium tip and outside the lamellipodium were not significantly different (tip: 16 ± 3 %; outside: 16 ± 3 %) (Figure 5E). Next we tested, if like Rac1, the activation state of RhoA was correlated with its selective immobilization in distinct regions of the lamellipodium. We applied the same strategy, using constitutively active (RhoA-Q63L) and inactive (RhoA-T19N) RhoA [50]. As opposed to Rac1-Q61L, active mEos2-RhoA-Q63L did not display selective immobilizations at the lamellipodium tip (tip: 27 ± 3 %; outside: 27 ± 2 %) (Figures 5B and E). This lack of selective immobilization was further reinforced by results obtained with inactive mEos2-RhoA-T19N, which displayed the same behavior as active RhoA-Q63L (Figures 5C and D-F). Active and inactive RhoA mutants displayed increased immobilization and slower free-diffusion compared to RhoA-WT both at the lamellipodium tip and outside of it (Figures 5E and F), potentially linked to increased interactions with GAPs, GEFs or effectors [51,52]. Thus, unlike Rac1, the activation state of RhoA does not control its immobilization at the lamellipodium tip. We also analyzed trajectories of Rac1 and RhoA wild-type and mutants in the core of the lamellipodium, i.e. between lamellipodium tip and outside (Data S1A, S4). However, the diffusive behaviors of proteins in the lamellipodium core and outside were similar, which confirms the selectivity of immobilization and decreased free-diffusion at the lamellipodium tip for active Rac1.

Transient and local Rac1 activations can trigger membrane protrusions

The smaller fraction of Rac1-WT immobilization at the lamellipodium tip compared to activated Rac1-Q61L indicated that dwell-times of interaction between activated Rac1-WT and effectors such as WRC are shorter than our acquisition frequency. Thus, we increased the acquisition frequency of sptPALM experiments from 50 Hz to 333 Hz to more efficiently capture transient Rac1-WT immobilizations [53]. The strong correlation between Rac1 activation and its selective immobilization at the lamellipodium tip was still observed at 333 Hz (Figures 6 and S4, Data S1C). Moreover, by increasing the acquisition frequency, we enhanced the disparity of diffusive behavior between Rac1-WT and active Rac1 mutants (Rac1-Q61L and Rac1-F28L) (Figures 6D-F, Video S2-S3). Indeed, the diffusive behavior of the fast cycling Rac1-F28L mutant, which was similar to Rac1-WT at 50 Hz (Figure 2), displayed a larger fraction of immobilization compare to Rac1-WT at 333 Hz (Figure 6E). Although we could capture seldom diffusion-trapping events of Rac1-WT at the lamellipodium tip (Video S2), even a frequency of 333 Hz was too slow to detect the bulk of Rac1-WT immobilizations. This suggests that most Rac1-effector interactions at the lamellipodium tip are transient and less than a few dozen milliseconds long.

To test how the subcellular location of Rac1 activation controls the formation of the lamellipodium, we used local, optogenetic activation of Rac1-WT. Light-induced interaction of the Cryptochrome CRY2 to its membrane-anchored CIBN partner was used to spatially and temporally control the

recruitment to the plasma membrane of cytosolic Rho-GEFs [54]. We applied the same strategy for Tiam1, a Rac1-GEF that also interacts with IRSp53 to promote WRC activation [41]. We used an optogenetic system composed of CIBN-GFP-CAAX localized at the cell membrane and Tiam1-CRY2-IRFP (Tiam1-CRY2), which is initially cytosolic (Figure 7A). Blue light illumination triggered fast and local membrane recruitment of Tiam1-CRY2 (Figures 7A-C, Video S4). We performed experiments after lamellipodia had already formed, illuminating regions either at the rear of lamellipodia or encompassing their tips (Figure 7D). When the region contained the lamellipodium tip, membrane recruitment of Tiam1-CRY2 rapidly increased the speed of protrusion (Figure 7E, Video S4). On the contrary, stimulation of membrane protrusion was inefficient when the illuminated region was located ~3 µm away from the tip (Figure 7E), despite efficient Tiam1-CRY2 membrane translocation. These results suggest that Rac1 activation should occur close to its effectors at the lamellipodium tip, and that inactivation of Rac1 occurs rapidly beyond the illuminated region.

To obtain more insight into the diffusive behavior of activated Rac1, independently from the use of constitutively active mutants, we combined optogenetic activation of Rac1-WT with simultaneous tracking of mEos2-Rac1-WT (Figures 7F-I). Sequences of mEos2-Rac1-WT sptPALM (10 s, 50 Hz) were acquired in between blue light illumination of a region containing the lamellipodium tip (Figure 7F). Membrane re-localization of Tiam1-CRY2 immediately increased the speed of membrane protrusion, attesting enhanced, local Rac1-WT activation. Nevertheless, its diffusive properties inside the region of optogenetic activation were similar to outside (Figures 7G-I, Data S1A), and were closer to mEos2-Rac1-WT than to mEos2-Rac1-Q61L. Thus, these results suggest that transient and local activation of Rac1 is sufficient for stimulating membrane protrusion, without the need to clamp Rac1-WT in its activated state.

Serum-mediated Rac1 activation triggers selective lamellipodium tip immobilizations

Many studies exploring the effects of Rho GTPases signaling on cell protrusions were performed on polarized, migrating cells in the presence of serum [29,30,55]. Thus, to test whether the selective immobilization of activated Rac1 at the lamellipodium tip is only occurring during isotropic cell spreading, or is intrinsically associated with the formation of active lamellipodia, we performed the same experiments 4 hours after MEF spreading and in the presence of 2 % serum (Figure S5, Data S1A). As in serum-free and isotropic spreading conditions, constitutively active mEos2-Rac1-Q61L displayed selective immobilizations at the lamellipodium tip (Figure S5B). Importantly, the fraction of immobilization at the lamellipodium tip for mEos2-Rac1-WT was increased to 28 ± 5 % (Figure S5F) compared to 13 ± 1 % in serum-free and spreading conditions (Figure 2F). This result is consistent with growth factor activation of Rac1 [5], and strengthens the idea that activated Rac1 molecules are selectively immobilized at the lamellipodium tip. Again, in contrast to Rac1, we observed no increased immobilization of RhoA-WT or RhoA-Q63L at the lamellipodium tip compared to outside (Figures S5C-G). In conclusion, these results suggest that active lamellipodia are intrinsically characterized by selective Rac1 immobilizations at their tips.

Discussion

Sites of Rac1 activation may differ from sites of Rac1 action.

The tight spatiotemporal regulation of actin regulatory proteins gives rise to complex periodic patterns of lamellipodium protrusion and retraction during cell migration [17,18]. The formation of those periodic patterns results from a complex interplay between signaling and mechanical events. Mechanical events are mainly based on forces generated by the lamellipodium, and it is the periodic physical connection of lamellipodial actin to myosin and early adhesions that drives periodic contractions [16,17,56]. The results presented here support a model in which signaling events triggering Rac1 activation foster its binding to effectors, at least WRC, at the lamellipodium tip to trigger membrane protrusion. Selective immobilizations of activated Rac1 at the lamellipodium tip appear to be a hallmark of active lamellipodia. Indeed, we consistently found this result in spreading MEFs, and in polarized migrating MEFs and B16 melanoma cells. The central role of Rac in lamellipodium formation is further supported by the fact that fibroblasts or B16 melanoma cells lacking Rac1,2,3 do not form lamellipodia [7,44]. To correlate cell edge movements with signaling activities, FRET sensors were used to monitor Rho GTPase or PKA activations in relation to periods of cell edge protrusion and retraction [29,57]. The zone of maximal Rac1 activation was located at the lamellipodium rear and found to climax asynchronously with the onset of edge protrusion [29]. Instead, the zone of RhoA activation encompassed the cell edge and was synchronized with the onset of protrusion [29,30]. One way to resolve these contradictions is to consider that sites of Rac1 activation could be distinct from sites of Rac1 action. Indeed, signaling events can rapidly propagate within the cell, enabling local signals to have remote consequences. This idea is consistent with heat maps of Rac1 activation showing that gradients of Rac1 activation, albeit not maximal at the lamellipodium tip, is still elevated there, possibly triggering WRC activation [29,36]. Despite the potential function of RhoA in initiating membrane protrusion through formin-dependent F-actin nucleation and elongation [29,58], no selective immobilizations at the lamellipodium tip were detected for RhoA-WT and RhoA-Q63L. These data could be interpreted either as lack of RhoA-effector interactions at the lamellipodium tip or, alternatively, as being undetectable by current experimental setups due to their extremely transient nature (< 10 ms). Nevertheless, aside from the tip, constitutively active RhoA-Q63L displayed increased immobilizations both inside and outside the lamellipodium, suggesting activated RhoA molecules to indeed bind effectors in those regions.

Correlation between Rac1 activation and immobilization at the lamellipodium tip

All proteins are part of interaction hubs, which implies that their functions depend on binding events with hub members. Using sptPALM, we showed that integrin activation events are correlated with immobilizations triggered by interactions with intracellular activators and/or extracellular ligands [24,59]. The use of Rho GTPase loss- or gain-of-function mutants likely prolongs interaction times with effectors, GEFs and GAPs above the temporal resolution, enabling to capture binding events associated with protein function. Using this strategy, previous studies demonstrated that Rac1 activation is correlated with immobilization in integrin-dependent focal adhesions [45] or neuronal dendritic spines [26]. Our results using SPT and super-resolution microscopy show that activated Rac1-Q61L is selectively immobilized at the lamellipodium tip and displays a reduced rate of free-diffusion.

These selective immobilizations could be mediated by binding to components of integrin-dependent, adhesive structures. Indeed, enrichment of activated integrins at lamellipodia or their tips was previously described [35,60]. Thus, integrins could induce local Rac activation and effector binding by directing its membrane recruitment through dissociation from Rho-GDI [36,61]. Furthermore, Rac1-WT and constitutively active Rac1 display immobilizations in adhesive structures [45]. This is consistent with the localization of Rac1-GEFs in mature, but also in early, integrin-dependent adhesive structures [45,62,63]. Nevertheless, nascent adhesive structures are not directly initiated at lamellipodia tips, but ~400 nm behind [16]. Rac1-GEF interactions at the tip might thus be responsible for the decreased rate and fraction of free-diffusion observed for Rac1-WT. Nevertheless, dominant negative Rac1-T17N, which displays increased binding towards GEF, but abrogated effector or GAP binding, behaves like CAAX-control, exhibiting no immobilizations at the lamellipodium tip, suggesting that Rac1 GEFs are not concentrated there. Instead, our results point towards an involvement of the direct lamellipodial Rac effector, WRC (Figure 4) [44]. However, our results are not excluding that other actin regulators also contribute to immobilization of activated Rac1 at the lamellipodium tip, such as IRSp53 family members [9,41–43], lamellipodin [64] or, more indirectly factors like Ena/VASP proteins also known to interact with WRC [65].

Long or short range of Rac1 action?

A recent study using SPT showed that Rac1 membrane recruitment precedes GTP loading [66]. This suggests that activated Rac1 will mainly diffuse at the plasma membrane and not in the cytosol. The radius of Rac1 action on its targets after activation, i.e. GTP loading, will thus be timed by the rate of GTP hydrolysis, but also by the relative distance between sites of Rac1 activation and effectors. WRC activation at the lamellipodium tip could be triggered either by active Rac1 originating from the lamellipodium rear (long range), or Rac1 activated in the vicinity of the tip (short range). In the latter model (Figure 7J right), local Rac1 activation could be triggered by specific Rac1-GEFs residing at the lamellipodium tip, as suggested by Tiam1 binding to IRSp53 [41], or in earliest adhesive structures located less than half a micron away from the lamellipodium tip [16], as proposed for Tiam1 and β-Pix [62,63]. In the long-range model (Figure 7J left), Rac1 activation would occur remotely, e.g. at mature adhesion sites located behind the lamellipodium, implying that activated, GTP-bound Rac1 would travel at least 2 µm to reach its target [29]. To enable activated Rac1 to cross the lamellipodium by membrane free-diffusion, Rac1-WT must then be clamped in the active state for few seconds (since the median free-diffusion of Rac1-Q61L is 0.68 $\mu m^2.s^{-1}$ at 333 Hz). If that was the case, we would have expected diffusive behaviors of Rac1-WT and Rac1-Q61L to be identical within the lamellipodium, which was not the case. Furthermore, fostering Rac1-WT activation within specific regions using optogenetic activation did not increase fractions of immobilization or decrease Ddiff values to levels observed for constitutively active Rac1-Q61L. Thus, our results support the short-range model, in which Rac1 remains only transiently active (few dozen milliseconds), requiring its continuous activation in the vicinity of effectors, close to the lamellipodium tip, to reach them before inactivation. Consistent with this, local optogenetic Rac1 activation efficiently enhanced protrusion if the activation region comprised the lamellipodium tip, but not if it was restricted to the lamellipodium rear (~3 µm behind the edge).

Biochemical approaches and *in vitro* model systems using purified proteins dramatically improved our understanding of the assembly mechanisms of F-actin networks, ranging from their initiation to their dynamics and mechanical properties [2,8,31,67–69]. The challenge now is to understand their

precise spatiotemporal orchestration at the molecular level in cells and how this impacts on F-actin architecture and dynamics. Here, we unraveled the nanoscale dynamic organization of Rac1 in migrating cells, demonstrating that its transient immobilizations at lamellipodia tips are hallmarks of rapid effector interactions during activation cycles triggering membrane protrusion.

Acknowledgments:

We thank B. Tessier, R. Sterling, J. Carrere for technical assistance; M. Garcia, A. Gautreau, M. Lagardère, T. Orré for helpful discussions; C. Poujol, S. Marais (Bordeaux Imaging Center, BIC) for technical help; F. Cordelières (BIC) for support in kymograph analysis (Kymo Tool Box); A. Gautreau and J.J. Gautier for mEos2 constructs of actin regulators. We acknowledge financial support from the French Ministry of Research and CNRS, ANR grant Integractome (GG), ANR grant FastNano (GG), La Ligue Contre le Cancer (AM), Conseil Régional Aquitaine (AM), Fondation pour la Recherche Médicale (GG, AM), Fondation ARC (VM), and the Deutsche Forschungsgemeinschaft (grant GRK2223/1 to KR).

Author Contributions:

GG conceived and coordinated the study. AM, OR, KR, VM and GG conceptualized the experiments. AM performed the experiments on MEFs. AM and GG analyzed the data. OR and AC performed pilots experiments. MS and KR designed and characterized the cellular and molecular tools related to B16-F1 cells. AM and MS performed the experiments on B16-F1 cells. AR and MC developed the optogenetic experiments. FB, AR, MC and ZK designed and generated new protein constructs. JBS developed the analytical tools for sptPALM. AM and GG wrote the manuscript and supplements. All authors discussed the results and commented on the manuscript.

Declaration of Interests

The authors declare no competing interests.

Figure legends

Figure 1. Membrane free-diffusion and trapping of WRC and IRSp53 at the lamellipodium tip.

(A) Experimental and analysis work flow. **(B)** Super-resolution intensity image of mEos2-Abi1 in the lamellipodium of a spreading MEF obtained from a sptPALM acquisition (left) (inset: fluorescence image of α-actinin-GFP). Corresponding trajectories are color-coded to show their diffusion modes: diffusive (gray), confined (yellow) and immobile (red) (right). **(C)** Same as B for mEos2-IRSp53. (D) Same as B for mEos2-CAAX. **(E)** Distribution of LOG(D) at the lamellipodium tip (left) and outside (right), mean for cells. The grey areas including D values inferior to 0.011 $\mu m^2.s^{-1}$ correspond to immobile trajectories. **(F)** Fractions of diffusive, confined and immobile populations at the lamellipodium tip (left) and outside (right), mean ± SEM for cells. **(G)** Diffusion coefficient (D) for free-diffusive trajectories at the lamellipodium tip (left) and outside (right) were represented by box plots displaying the median (notch) and mean (square) ± percentile (25-75%). All results for each condition correspond to pooled data from several independent experiments. Where indicated, statistical significances were obtained using two-tailed, unpaired t-test for fractions of immobilization (E) or non-parametric, two-tailed Mann-Whitney rank sum test for diffusion coefficients (F). Inside the lamellipodium tip and outside the lamellipodium, all the different conditions were compared (black P-values). Inside the lamellipodium tip, each given condition was compared with the value obtained outside the lamellipodium (colored P-values). The resulting P-values are indicated as follows: ns, $P > 0.05$; *$P < 0.05$; ***$P < 0.001$. See also Figure S1, Data S1 and Video S1.

Figure 2. Correlation between Rac1 activation and transient immobilizations at the lamellipodium tip.

(A) Super-resolution intensity image of mEos2-Rac1-WT in the lamellipodium of a spreading MEF obtained from a sptPALM acquisition (left). Corresponding trajectories (right). **(B)** Same as A for mEos2-Rac1-Q61L. **(C)** Same as A for mEos2-Rac1-T17N. **(D)** Same as A for mEos2-Rac1-F28L. **(E)** Distribution of LOG(D) at the lamellipodium tip (top) and outside (bottom), mean for cells. **(F)** Fractions of diffusive, confined and immobile populations at the lamellipodium tip (left) and outside (right), mean ± SEM for cells. **(G)** Diffusion coefficients (D) for free-diffusive trajectories at the lamellipodium tip (left) and outside (right). All results for each condition correspond to pooled data from several independent experiments. At the lamellipodium tip and outside the lamellipodium, all the different conditions were compared to the Rac1-WT condition (black P-values). At the lamellipodium tip, each given condition was compared with the value obtained outside the lamellipodium (colored P-values). See also Figures S5 and S6 and Data S1.

Figure 3. Immobilization of active Rac1 at the lamellipodium tip depends on binding to effectors involved in lamellipodium formation.

(A) Super-resolution intensity image of mEos2-Rac1-Y40C in the lamellipodium of a spreading MEF obtained from a sptPALM acquisition (left). Corresponding trajectories (right). **(B)** Same as A for mEos2-Rac1-Y40C-Q61L. **(C)** Same as A for mEos2-Rac1-F37A. **(D)** Same as A for mEos2-Rac1-F37A-Q61L. **(E)** Distribution of LOG(D) at the lamellipodium tip (top) and outside (bottom), mean for cells. **(F)** Fractions of diffusive, confined and immobile populations at the lamellipodium tip (left) and outside (right), mean ± SEM for cells. **(G)** Diffusion coefficients (D) for free-diffusive trajectories at the lamellipodium tip (left) and outside (right). All results for each condition correspond to pooled data from several independent experiments. At the lamellipodium tip and outside the lamellipodium, conditions were compared to the Rac1-WT condition or the Rac1-Q61L condition (black P-values). At the lamellipodium tip, each given condition was compared with values obtained outside the lamellipodium (colored P-values). See also Data S1.

Figure 4. Activated Rac1 immobilization at the lamellipodium tip depends on its interaction with WRC.

(A) Super-resolution intensity image of mEos2-Rac1-WT in the lamellipodium of B16 Sra1/PIR121-KO cell co-transfected with Sra1-WT-GFP obtained from a sptPALM acquisition (left). Corresponding trajectories (right). **(B)** Same as A for mEos2-Rac1-Q61L co-transfected with Sra1-WT-GFP. **(C)** Same as A for mEos2-Rac1-Q61L co-transfected with Sra1-WCA*-GFP. **(D)** Same as A for mEos2-Rac1-F37A-Q61L co-transfected with Sra1-WCA*-GFP. **(E, G)** Distribution of LOG(D) at the lamellipodium tip, mean for cells. **(F, H)** Fractions of immobilization at the lamellipodium tip (medians (black lines) and arithmetic means (black squares)). **(I)** Fractions of diffusive, confined and immobile populations at the lamellipodium tip, mean ± SEM for cells. **(J)** Diffusion coefficients (D) for free-diffusive trajectories at the lamellipodium tip. All results for each condition correspond to pooled data from several independent experiments. **(K)** Fluorescence image of Sra1-WT-GFP in a B16 Sra1/PIR121-KO co-transfected with mEos2-Rac1-Q61L (left). Kymographs generated from a sptPALM acquisition (50 Hz) to measure mEos2-Rac1-Q61L immobilization times at the lamellipodium tip (as shown in the left panel, dashed lines). **(L)** Same as K in Sra1-WCA*-GFP condition. **(M)** Immobilization times (>260 ms) at the lamellipodium tip in Sra1-WT-GFP (364 events / 8 cells) and Sra1-WCA*-GFP (495 events / 6 cells) conditions (medians (notch) and arithmetic means (squares) ± percentiles (25-75%)). Statistical significance was obtained using non-parametric, two-tailed Mann-Whitney rank sum test for immobilization time (M). See also Figures S2 and S3 and Data S1.

Figure 5. RhoA activation level is not correlated with immobilizations in specific, lamellipodial regions.

(A) Super-resolution intensity image of mEos2-RhoA-WT in the lamellipodium of a spreading MEF obtained from a sptPALM acquisition (left). Corresponding trajectories (right). **(B)** Same as A for mEos2-RhoA-Q63L. **(C)** Same as A for mEos2-RhoA-T19N. **(D)** Distribution of LOG(D) at the lamellipodium tip (left) and outside (right), mean for cells. **(E)** Fractions of diffusive, confined and

immobile populations at the lamellipodium tip (left) and outside (right), mean ± SEM for cells. **(F)** Diffusion coefficients (D) for free-diffusive trajectories at the lamellipodium tip (left) and (right). All results for each condition correspond to pooled data from several independent experiments. Inside the lamellipodium tip and outside the lamellipodium, all the different conditions were compared to the RhoA-WT condition (black P-values). Inside the lamellipodium tip, each given condition was compared with the value obtained outside the lamellipodium (colored P-values). See also Figures S5 and S6 and Data S1.

Figure 6. Distinct diffusive behaviors of Rac1-WT, Rac1-F28L and Rac1-Q61L revealed by fast acquisition frequencies.

(A) Super-resolution intensity image of mEos2-Rac1-WT in the lamellipodium of a spreading MEF obtained from a sptPALM acquisition (left) (333 Hz, duration: 12 s; inset: fluorescence image of α-actinin-GFP). Corresponding trajectories (right). **(B)** Same as A for mEos2-Rac1-Q61L. **(C)** Same as A for mEos2-Rac1-F28L. **(D)** Distribution of LOG(D) at the lamellipodium tip (left) and outside (right), mean for cells. The grey areas including D values inferior to 0.052 $\mu m^2.s^{-1}$ correspond to immobile trajectories. **(E)** Fractions of diffusive, confined and immobile populations at the lamellipodium tip (left) and outside (right), mean ± SEM for cells. **(F)** Diffusion coefficients (D) for free-diffusive trajectories at the lamellipodium tip (left) and outside (right). All results for each condition correspond to pooled data from several independent experiments. Inside the lamellipodium tip and outside the lamellipodium, all the different conditions were compared to the Rac1-WT condition (black P-values). Inside the lamellipodium tip, each given condition was compared with the value obtained outside the lamellipodium (colored P-values). See also Figure S4, Data S1 and Videos S2 and S3.

Figure 7. Transient and local Rac1 activations are able to trigger membrane protrusions.

(A) Schematic of Rac1 optogenetic activation. **(B)** TIRF images of Tiam1-CRY2-IRFP before (left) and after (right) photoactivation. **(C)** Normalized increase of Tiam1-CRY2-IRFP fluorescence in the photoactivated region or outside during photoactivation (gray area). **(D)** Schematic of photoactivated areas encompassing the lamellipodium tip (Photoac. Tip) and 3 µm away from the lamellipodium tip (Photoac. Rear). **(E)** Lamellipodium protrusion as a function of time before and during photoactivation (gray area) (left). Protrusion speed during photoactivation for the area encompassing the lamellipodium tip and the area away from the lamellipodium tip (right). Protrusion speeds were measured in front of photoactivated areas (plain lines) and in control parts of the cells (dotted lines), as depicted in (D). **(F)** Super-resolution intensity image obtained from a sptPALM acquisition of mEos2-Rac1-WT in the lamellipodium of a spreading MEF after optogenetic membrane recruitment of Tiam1-CRY2-IRFP (left) (same cell as B). Corresponding trajectories (right). **(G)** Distribution of LOG(D) inside and outside the photoactivated region, mean for cells. **(H)** Fractions of diffusive, confined and immobile populations inside and outside the photoactivated region, mean ± SEM for cells. **(I)** Diffusion coefficients (D) for free-diffusive trajectories inside and outside the photoactivated region. All results for each condition correspond to pooled data from several independent experiments. Statistical significance was obtained using non-parametric, two-tailed

Mann-Whitney rank sum test for protrusion speeds (E). **(J)** Schematic representation of alternative working models. See also Figure S7, Data S1 and Video S4.

STAR Methods

LEAD CONTACT AND MATERIALS AVAILABILITY

Further information and requests for resources and reagents should be directed to and will be fulfilled by the Lead Contact, Grégory Giannone (gregory.giannone@u-bordeaux.fr). Plasmids generated in this study have not been deposited to Addgene and should be requested to the Lead Contact, Grégory Giannone (gregory.giannone@u-bordeaux.fr). B16-F1 Sra-1/PIR121 KO and B16-F1 Rac1/2/3 KO cell lines should be requested to Klemens Rottner (k.rottner@tu-braunschweig.de).

EXPERIMENTAL MODEL AND SUBJECT DETAILS

B16-F1 (from ATCC/CRL-6323, sex: male) melanoma cells disrupted for Sra-1 and PIR121 were a gift from Dr Klemens Rottner's Lab.

Mouse Embryonic Fibroblasts (MEFs) were immortalized and described in Su J, Muranjan M, Sap J. (1999). Primary embryonic fibroblasts were isolated from E13–E15 day old RPTPα+/+ embryos and immortalized using a retroviral vector expressing polyoma large T antigen.

MEFs and B16-F1 cells were cultured in DMEM (4.5 g/l glucose, free from L-Glutamine, with Sodium Pyruvate), supplemented with 10% Fetal Bovine Serum (FBS), 2 mM glutamine, penicillin (10 Units/ml)/streptomycin (100 µg/ml) and 15 mM HEPES. The authentication was performed by the laboratory responsible for the cell line generation. The cell lines used in this study were frequently tested for Mycoplasma and they have all been verified as Mycoplasma free.

METHOD DETAILS

Cell culture and spreading assays

For MEFs, transient transfections of plasmids were performed 2 days before experiments using Amaxa Nucleofector (Lonza). Cells were detached with trypsin/EDTA (0.05% for 2 min), and after trypsin inactivation with soybean trypsin inhibitor (1 mg/ml in DMEM), washed and suspended in serum-free Ringer, followed by incubation for 30 min before spreading on human FN (Roche)-coated glass surface (FN 10µg/ml) [16,17]. For experiments performed on polarized MEFs in the presence of serum, 4 hours before experiments, cells were detached with trypsin/EDTA (0.05% for 2 min), suspended and allowed to spread in Ringer with 2 % of FBS on human FN (Roche)-coated glass surface (FN 10µg/ml).

For B16-F1, transient transfections of plasmids were performed 2 days before experiments using Amaxa Nucleofector (Lonza). Four hours before experiments, the cells were detached with trypsin/EDTA (0.05% for 2 min), the trypsin inactivated using soybean trypsin inhibitor (1 mg/ml in DMEM), and the cells washed, suspended and allowed to spread in serum-free Ringer on laminin (LM) (Sigma)-coated glass surface (LM 25µg/ml).

DNA constructs

mEos2-Abi1, mEos2-IRSp53, mEos2-CAAX, mEos2-Rac1-WT, mEos2-Rac1-Q61L, mEos2-Rac1-T17N, mEos2-Rac1-F28L were generated by PCR of the coding DNA sequence of the corresponding protein and inserted into the pcDNAm-FRT-PC-mEos2 blue vector at Fse1/Asc1 sites. mEos2-Rac1-F37A, mEos2-Rac1-Y40C, mEos2-Rac1-Q61L-F37A and mEos2-Rac1-Q61L-Y40C were generated by mutagenesis, respectively, in the pcDNAm-FRT-PC-mEos2-Rac1-WT and pcDNAm-FRT-PC-mEos2-Rac1-Q61L vector. mEos2-RhoA-WT, mEos2-RhoA-Q63L and mEos2-RhoA-T19N were generated by PCR from, respectively, pGEX-RhoA, RhoA-Q63L and RhoA-T19N, and cloned into the pmEos2-C1 vector using BglII/XhoI sites. CIBN-GFP-CAAX was described previously [54] and CRY2PHR-Tiam1-iRFP was obtained using the strategy described in [54]. α-actinin-GFP construct was described previously [17]. pEGFP-C2-Sra1 variants, pmCherry-C2-Sra1-WT, pEGFP-C1-Rac1-Q61L, and pEGFP-C1-Rac1-F37A-Q61L were described previously [44]. pmCherry-C2-Sra-1-WCA* was generated by swapping EGFP with mCherry, kindly provided by Dr. Roger Tsien (University of California at San Diego, La Jolla, California, USA) using NheI/BsrGI restriction sites. The fidelity of all constructs was verified by sequencing.

Immunoprecipitation

For EGFP-immunoprecipitation experiments, Sra1/PIR121 KO cells (clone #3) co-expressing EGFP alone or EGFP-Rac1-Q61L or EGFP-Rac1-F37A-Q61L together with mCherry-tagged Sra1 variants were lysed with lysis buffer on ice (1% Triton X-100, 140 mM KCl, 50 mM Tris/HCl pH 7.4/ 50 mM NaF, 10 mM $Na_4P_2O_7$, 2 mM $MgCl_2$ and Complete Mini, EDTA-free protease inhibitor [Roche]). The following steps were carried out on ice: Lysates were cleared at 16,000 g for 10 min and incubated with GFP-Trap agarose beads for 60 min. Subsequently, beads were washed three times with lysis buffer lacking Triton X-100 and protease inhibitor, mixed with Laemmli buffer, boiled for 5 min and subjected to Western Blotting.

SptPALM acquisitions

Cells were imaged at 37°C in a Ludin chamber (Life Imaging Services) with an inverted motorized microscope (Nikon Ti) equipped with a CFI Apo TIRF 100x oil, NA 1.49 objective and a perfect focus system, allowing long acquisition in TIRF illumination mode. For photoactivation localization microscopy, cells expressing mEos2 tagged constructs were photoconverted using a 405 nm laser (Omicron) and the resulting photoconverted single molecule fluorescence was excited with a 561 nm laser (Cobolt Jive™). Both lasers illuminated the sample simultaneously. Their respective power was adjusted to keep the number of stochastically activated molecules constant and well separated during acquisition. Fluorescence was collected by the combination of a dichroic and emission filters (dichroic: Di01-R561, emission: FF01-617/73, Semrock) and a sensitive EMCCD (Electron-Multiplying Charge-Coupled Device, Evolve, Photometric) for 50 Hz acquisitions or a sCMOS (scientific Complementary Metal-Oxide Semiconductor, Orca Flash4, Hamamatsu) for 333 Hz acquisitions. The acquisition was steered by Metamorph software (Molecular Devices) in streaming mode. α-actinin-GFP was imaged using a conventional GFP filter cube (excitation: FF01-472/30, dichroic: FF-495Di02, emission: FF01-520/35). Using this filter cube does not allow to separate spectrally the unconverted pool of mEos2 from the GFP fluorescent signal. However, with all the constructs used, whether the mEos2 signal was highly or poorly enriched in lamellipodium, we were still able to detect lamellipodia with α-actinin-GFP.

Since high levels of expression of Rho GTPase mutants might affect lamellipodia formation, dynamics and morphologies [51,52], we performed acquisitions only on cells able to spread and polarize, and in the absence of dramatic phenotypes such as (1) being unable to spread but forming membrane tubules (high levels of RhoA-Q63L expression), (2) bearing numerous lamellipodia (high levels of Rac1-Q61L). Instead, we analyzed cells displaying an active, protrusive lamellipodium, in phase 2 of spreading (according to [16,17]). To test that we were not performing experiments on cells having aberrant protrusive behaviors, we also measured rates of lamellipodium protrusion for the cells used for sptPALM analysis (Figure S6A). The rates of protrusion for the cells analyzed in different conditions were not dramatically different among another (Figure S6A). This suggests that, in our acquisition conditions, levels of expression of distinct mEos2-fused proteins were not triggering dramatic effects on lamellipodium protrusion. In addition, to further support that the specific diffusive behaviors we observed for each Rho GTPase (wild-type and mutants) were independent from expression levels of various mEos2-fused proteins, we plotted the fraction of immobilizations as function of the density of trajectories (Figures S6B-G). We observed no correlation between density of trajectories and fraction of immobilizations. For example, mEos2-Rac1-Q61L (Figure S6C) displayed a larger fraction of immobilization compared to mEos2-Rac1-WT (Figure S6B) for low and high densities of trajectories.

Single molecule segmentation and tracking

A typical sptPALM acquisition generates between 4000-7500 images per cell analyzed in order to extract molecule localization and dynamics. Single molecule fluorescent spots were localized and tracked over time using a combination of wavelet segmentation and simulated annealing algorithms [34,71]. Under the experimental conditions described above, the resolution of the system was quantified to 59 nm (50 Hz, EMCCD), 49 nm (333 Hz, sCMOS) (Full Width at Half Maximum, FWHM). This spatial resolution depends on the image signal to noise ratio and the segmentation algorithm and was determined using fixed mEos2 samples. We analyzed 2D distributions of single molecule positions belonging to long trajectories (>50 frames) by bi-dimensional Gaussian fitting, the resolution being determined as $2.3s_{xy}$, where s_{xy} is the pointing accuracy.

For the trajectory analysis, lamellipodia tips were identified by thresholding fluorescence signals of α-actinin-GFP images acquired in between sptPALM sequences (1500 images at 50 Hz and 400 images at 333 Hz). The cell edge for each α-actinin-GFP image was detected. For consecutive images, localized edges were extended by 3 pixels (480 nm) outside of the cell for the distal edge and inside the cell for the proximal edge, delimiting the area explored by the lamellipodium tip during the sptPALM sequence recorded in between. This allowed to keep the protruding lamellipodium tip within the region of interest during sptPAM sequences. The region outside the lamellipodium was defined as the region 25 pixels (4 µm) inward from the distal edge. The corresponding binary masks were used to sort single particle data analyses to specific regions, lamellipodium tip, outside the lamellipodium. We analyzed trajectories lasting at least 13 points (≥ 260 ms, 50 Hz ; ≥ 39 ms, 333 Hz) with a custom routine written for Matlab using the mean squared displacement MSD computed as (Eq. 1):

$$MSD(t = n \cdot \Delta t) = \frac{\sum_{i=1}^{N-n}(x_{i+n} - x_i)^2 + (y_{i+n} - y_i)^2}{N - n} \qquad Eq.1$$

where x_i and y_i are the coordinates of the label position at time $i \cdot \Delta t$. We defined the measured diffusion coefficient D as the slope of the affine regression line fitted to the $n = 1$ to 4 values of

the $MSD(n \cdot \Delta t)$. The MSD was computed, and then fitted on a duration equal to 80% (minimum of 10 points, 200 ms (50 Hz), 30 ms (333 Hz)) of the whole stretch by (Eq 2):

$$MSD(t) = \frac{4r_{conf}^2}{3}\left(1 - e^{-t/\tau}\right) \qquad Eq.2$$

where r_{conf} is the measured confinement radius and τ the time constant ($\tau = r_{conf}^2/3D_{conf}$). To reduce the inaccuracy of the MSD fit due to down sampling for larger time intervals, we used a weighted fit. Trajectories were sorted into 3 groups: immobile, confined diffusion and free-diffusion. Immobile trajectories were defined as trajectories with D<0.011 $\mu m^2.s^{-1}$ (50 Hz), D<0.052 $\mu m^2.s^{-1}$ (333 Hz), corresponding to molecules that explored an area inferior to the one defined by the image spatial resolution ~(0.059 µm)^2 at 50 Hz ~(0.049 µm)^2 at 333 Hz during the time used to fit the initial slope of the MSD [24]. For the EMCCD experiments performed at 50 Hz, 4 points, 80 ms: $D_{threshold}$=(0.059 µm)^2/(4x4x0.02 s)~0.011 $\mu m^2.s^{-1}$. For the sCMOS experiments performed at 333 Hz, 4 points, 12 ms: $D_{threshold}$=(0.059 µm)^2/(4x4x0.003 s)~0.052 $\mu m^2.s^{-1}$. To separate trajectories displaying free-diffusion from confined diffusion, we used the time constant τ calculated for each trajectory. Confined and free-diffusing trajectories were defined as trajectories with a time constant τ respectively inferior and superior to half the time interval used to compute the MSD (100 ms (50 Hz); 15 ms (333 Hz)). Cells were excluded from the analysis if SPT acquisitions yielded less than 50 trajectories per region of interest: lamellipodium tip and outside of the lamellipodium. The values for all physical parameters (fraction and diffusion coefficients of diffusive, confined and immobile trajectories, and confinement radius) in each condition are plot in Data S1

Kymograph generation and analysis

Kymographs were generated and analyzed using an ImageJ plugin, Kymo ToolBox (F. Cordelières) on sptPALM fast acquisition frequency images (50 Hz; 7500 frames). Kymographs were generated from lines of interest (LOI) tangential to the lamellipodium tip. Kymographs were analyzed after manual annotation, enabling Kymo ToolBox to extract the duration of Rac1 immobilizations. Only immobilizations longer than 260 ms were used for quantification of immobilization time.

Optogenetic activation of Rac1 using Tiam1 membrane recruitment

MEFs were co-transfected with CIBN-GFP-CAAX, Tiam1-CRY2-IRFP and mEos2-Rac1-WT. TIRF images of spreading MEFs were acquired using an azimuthal TIRF module (ilas2; Roper Scientific, Tucson, AZ), and laser power and exposure times chosen to limit phototoxicity potentially interfering with cell edge protrusion. To photoactivate CRY2, we used a fluorescence recovery after photobleaching (FRAP) head (Roper Scientific) to illuminate with the 488 nm laser in defined regions of interest. Tiam1-CRY2-IRFP images were acquired every 20 s. After a base line of Tiam1-CRY2-IRFP images (4 images), Tiam1-CRY2-IRFP acquisitions were preceded by CRY2 photoactivation (~ 500 ms). sptPALM sequences of mEos2-Rac1-WT (10 s, 500 images, 50 Hz) were acquired in between CRY2 photoactivation. This procedure was repeated for at least 15 times.

This imaging protocol triggered increased densities of mEos2-Rac1-WT trajectories in regions of interest (Figure 7). To test that these increased densities were independent from Tiam1-CRY2-IRFP membrane recruitment and enhanced Rac1 activation, we performed control experiments in MEFs that did not express the optogenetic actuator (Tiam1-CRY2-IRFP) (Figure S10). Like in conditions where Tiam1-CRY2-IRFP is expressed, we also observed increased densities of trajectories in regions of interest used for optogenetic activation (Figure S7). The diffusive properties of mEos2-Rac1-WT

inside regions of optogenetic activation were also similar to outside (Figure S7) and closer to mEos2-Rac1-WT than to mEos2-Rac1-Q61L (Figure S7). Cells were excluded from the analysis if the photoactivation was not followed by a local membrane recruitment of Tiam1-CRY2.

Measurements of lamellipodium protrusion speeds (Figure 7E) were performed using kymographs (ImageJ plugin, Kymo ToolBox, F. Cordelières). We first generated Tiam1-CRY2-IRFP time-lapse sequences (Video S4). Then, Kymo ToolBox was used to generate kymographs from lines perpendicular to the lamellipodium tip in front of the photoactivated area or perpendicular to a control part of the cell (Figure 7D). Then, lines were manually generated on kymographs, and Kymo ToolBox extracted the displacements and the speed of cell edges.

QUANTIFICATION AND STATISTICAL ANALYSIS

All results for each condition correspond to datasets from at least three independent experiments and were not analyzed in blind conditions. All experimental conditions (cell transfection, delay between transfection and imaging, cell density) were carefully normalized to minimize variability. No statistical calculations were used to predict the sample size.

For single molecule tracking experiments we imaged between 5 to 30 cells per condition. Each cell was analyzed independently and the distributions of the diffusion coefficients were computed from 6 000-150 000 trajectories (Figures 1-7 and S3, 5, 7, Data S1). The statistical n for the fractions of trajectories in the different diffusion modes (immobile, confined, free-diffusive) correspond to the number of analyzed cells (Figures 1-7 and S3, 5, 7, Data S1). Statistical n for diffusion coefficient correspond to the number of trajectories (Figures 1-7 and S3, 5, 7, Data S1). Statistical n for the ratio between the detection density inside and outside the photoactivated area correspond to the number of analyzed cells (Figure S7E).

For the kymograph analysis of the mEos2-Rac1-Q61L immobilization time at the lamellipodium tip, we imaged 8 and 6 cells respectively in Sra1-WT-GFP and Sra1-WCA*-GFP condition, generating respectively 364 and 495 events per condition (Figures 4K-M). Statistical n for the immobilization times correspond to the number of events (Figure 4M).

For the analysis of the lamellipodium protrusion after photoactivation, we imaged 8 cells with photoactivated areas containing the lamellipodium tip and 3 cells with photoactivated areas 3 µm away from the lamellipodium tip (Figures 7D-E), generating respectively 133 and 59 steps of protrusion measurements both in front of the photoactivated areas and in a control part of the cells (Figures 7D-E). Statistical n for the protrusion speeds correspond to the number of protrusion steps measured (Figure 7E).

For the quantification of the rescue of the lamellipodia formation, we imaged from 158 to 250 cells per condition (Figures S2A-B), the statistical n correspond to the number of analyzed cells (Figure S2B).

The statistical significances associated with the fractions of immobilization were obtained using two-tailed unpaired t-test (Figures 1-7 and S3, 5, 7, Data S1). The statistical significances associated with the diffusion coefficients (Figures 1-7 and S3, 5, 7, Data S1), the immobilization times of mEos2-Rac1-Q61L at the lamellipodium tip (Figure 4M), the speed of protrusion after photoactivation (Figure 7E)

and the ratio between the detection density inside and outside the photoactivated areas (Figure S7E) were obtained using a non-parametric, two-tailed Mann-Whitney rank sum test. The statistical significances associated with the quantification of the rescue of the lamellipodia formation (Figure S2B) were obtained using a t-test. The resulting P values are indicated as follows: NS: $P > 0.05$; *: $0.01 < P < 0.05$; **: $0.001<P<0.01$; ***: $P<0.001$; ****: $P < 0.0001$. All Statistical analyses were performed using GraphPad Prism software version 5.03 for Windows (GraphPad Software, La Jolla California USA, www.graphpad.com).

DATA AND CODE AVAILABILITY

The published article includes all datasets generated or analyzed during this study

Supplemental data file

Data S1. Results obtained using sptPALM acquisitions and statistics. Related to STAR Methods, Figures 1-7 and Figure S3-S5, 7.

(A) Results obtained using sptPALM acquisitions at 50 Hz in MEFs. Related to Figures 1-3, 5, 7 and S5, S7. Several physical parameters (fraction and diffusion coefficients of diffusive, confined and immobile trajectories, and confinement radius) were obtained from lamellipodium of MEF cells in different experimental conditions (spreading, polarized migrating cells in the presence of serum, and under optogenetic manipulation) and were measured in different locations (tip, core and outside of the lamellipodium). The values correspond to Mean ± SEM. **(B)** Results obtained using sptPALM acquisitions at 50 Hz in B16 cells. Related to Figures 4 and S3. Several physical parameters (fraction and diffusion coefficients of diffusive, confined and immobile trajectories, and confinement radius) were obtained in the lamellipodium of polarized migrating B16 cells and were measured in different locations (tip and outside of the lamellipodium). The values correspond to Mean ± SEM. **(C)** Results obtained using sptPALM acquisitions at 333 Hz in MEFs. Related to Figures 6 and S4. Several physical parameters (fraction and diffusion coefficients of diffusive, confined and immobile trajectories, and confinement radius) were obtained in the lamellipodium of spreading MEF and were measured in different locations (tip and outside of the lamellipodium). Images were acquired by sptPALM at 333 Hz. The values correspond to Mean ± SEM. **(D)** Summary statistics for results obtained using sptPALM acquisitions at 50 Hz in MEFs. Related to Figures 1-3, 5, 7 and S5, S7. **(E)** Summary statistics for results obtained using sptPALM acquisitions at 50 Hz in B16 cells. Related to Figures 4 and S3. **(F)** Summary statistics for results obtained using sptPALM acquisitions at 333 Hz in MEFs. Related to Figures 6 and S4.

Supplemental video

Video S1. From raw sptPALM acquisitions to super-resolution intensity images and trajectories. Related to Figure 1.
(**A)** Raw acquisition of mEos2-Abi1 from one sptPALM sequence (50 Hz). **(B)** Localization of single molecule fluorescent spots. **(C)** Corresponding super-resolution intensity image. **(D)** Corresponding trajectories are color-coded to show their diffusion modes: diffusive (gray), confined (yellow) and immobile (red). Scale bars, 2 µm.

Video S2. Rare diffusion-trapping events of Rac1-WT at the lamellipodium tip. Related to Figure 6.
(**A)** Fluorescence image of α-actinin-GFP. Scale bars, 2 µm. **(B)** Raw acquisition of mEos2-Rac1-WT from one sptPALM sequence (333 Hz, duration: 1.2s). Lines were added to distinguish the lamellipodium tip. Arrowheads highlight immobilization events. Scale bars, 2 µm.

Video S3. Diffusion-trapping events of Rac1-Q61L at the lamellipodium tip. Related to Figure 6.
(A) Fluorescence image of α-actinin-GFP. Scale bars, 2 µm. **(B)** Raw acquisition of mEos2-Rac1-Q61L from one sptPALM sequence (333 Hz, duration: 1.2s). Lines were added to distinguish the lamellipodium tip. Arrow heads highlight immobilization events. Scale bars, 2 µm.

Video S4. Stimulation of lamellipodium protrusion by Tiam1-CRY2-IRFP membrane recruitment. Related to Figure 7.
Time-lapse of Tiam1-CRY2-IRFP photoactivation sequences (20 s). After a base line of 4 images, a region encompassing the lamellipodium tip is photoactivated every 20 s by low 488 nm laser illumination triggering recruitment of Tiam1-CRY2-IRFP to the plasma membrane and lamellipodium protrusion. Scale bars, 15 µm.

References

1. Bravo-Cordero, J.J., Hodgson, L., and Condeelis, J. (2012). Directed cell invasion and migration during metastasis. Curr. Opin. Cell Biol. *24*, 277–83.

2. Blanchoin, L., Boujemaa-Paterski, R., Sykes, C., and Plastino, J. (2014). Actin dynamics, architecture, and mechanics in cell motility. Physiol. Rev. *94*, 235–63.

3. Krause, M., and Gautreau, A. (2014). Steering cell migration: lamellipodium dynamics and the regulation of directional persistence. Nat. Rev. Mol. Cell Biol. *15*, 577–590.

4. Heasman, S.J., and Ridley, A.J. (2008). Mammalian Rho GTPases: New insights into their functions from in vivo studies. Nat. Rev. Mol. Cell Biol. *9*, 690–701.

5. Ridley, A.J., Paterson, H.F., Johnston, C.L., Diekmann, D., and Hall, A. (1992). The small GTP-binding protein rac regulates growth factor-induced membrane ruffling. Cell *70*, 401–410.

6. Wu, Y.I., Frey, D., Lungu, O.I., Jaehrig, A., Schlichting, I., Kuhlman, B., and Hahn, K.M. (2009). A genetically encoded photoactivatable Rac controls the motility of living cells. Nature *461*, 104–108.

7. Steffen, A., Ladwein, M., Dimchev, G. a, Hein, A., Schwenkmezger, L., Arens, S., Ladwein, K.I., Margit Holleboom, J., Schur, F., Victor Small, J., *et al.* (2013). Rac function is crucial for cell migration but is not required for spreading and focal adhesion formation. J. Cell Sci. *126*, 4572–88.

8. Chen, Z., Borek, D., Padrick, S.B., Gomez, T.S., Metlagel, Z., Ismail, A.M., Umetani, J., Billadeau, D.D., Otwinowski, Z., and Rosen, M.K. (2010). Structure and control of the actin regulatory WAVE complex. Nature *468*, 533–538.

9. Miki, H., Yamaguchi, H., Suetsugu, S., and Takenawa, T. (2000). IRSp53 is an essential intermediate between Rac and WAVE in the regulation of membrane ruffling. Nature *408*, 732–735.

10. Breitsprecher, D., Kiesewetter, A.K., Linkner, J., Urbanke, C., Resch, G.P., Small, J.V., and Faix, J. (2008). Clustering of VASP actively drives processive, WH2 domain-mediated actin filament elongation. EMBO J *27*, 2943–2954.

11. Block, J., Breitsprecher, D., Kühn, S., Winterhoff, M., Kage, F., Geffers, R., Duwe, P., Rohn, J.L., Baum, B., Brakebusch, C., *et al.* (2012). FMNL2 drives actin-based protrusion and migration downstream of Cdc42. Curr. Biol. *22*, 1005–12.

12. Mejillano, M.R., Kojima, S., Applewhite, D.A., Gertler, F.B., Svitkina, T.M., and Borisy, G.G. (2004). Lamellipodial versus filopodial mode of the actin nanomachinery: pivotal role of the filament barbed end. Cell *118*, 363–73.

13. Lai, F.P.L., Szczodrak, M., Block, J., Faix, J., Breitsprecher, D., Mannherz, H.G., Stradal, T.E.B., Dunn, G.A., Small, J.V., and Rottner, K. (2008). Arp2/3 complex interactions and actin network turnover in lamellipodia. EMBO J *27*, 982–992.

14. Wilson, C.A., Tsuchida, M.A., Allen, G.M., Barnhart, E.L., Applegate, K.T., Yam, P.T., Ji, L., Keren, K., Danuser, G., and Theriot, J.A. (2010). Myosin II contributes to cell-scale actin network treadmilling through network disassembly. Nature *465*, 373–377.

15. Iwasa, J.H., and Mullins, R.D. (2007). Spatial and temporal relationships between actin-filament nucleation, capping, and disassembly. Curr. Biol. *17*, 395–406.

16. Giannone, G., Dubin-Thaler, B.J., Rossier, O., Cai, Y., Chaga, O., Jiang, G., Beaver, W., Döbereiner, H.G., Freund, Y., Borisy, G., *et al.* (2007). Lamellipodial Actin Mechanically Links

Myosin Activity with Adhesion-Site Formation. Cell *128*, 561–575.

17. Giannone, G., Dubin-Thaler, B.J., Döbereiner, H.-G., Kieffer, N., Bresnick, A.R., and Sheetz, M.P. (2004). Periodic lamellipodial contractions correlate with rearward actin waves. Cell *116*, 431–43.

18. Ponti, a, Machacek, M., Gupton, S.L., Waterman-Storer, C.M., and Danuser, G. (2004). Two distinct actin networks drive the protrusion of migrating cells. Science (80-.). *305*, 1782–1786.

19. Liu, Z., Lavis, L.D., and Betzig, E. (2015). Imaging Live-Cell Dynamics and Structure at the Single-Molecule Level. Mol. Cell *58*, 644–659.

20. Sahl, S.J., Hell, S.W., and Jakobs, S. (2017). Fluorescence nanoscopy in cell biology. Nat. Rev. Mol. Cell Biol. *18*, 685–701.

21. Manley, S., Gillette, J.M., Patterson, G.H., Shroff, H., Hess, H.F., Betzig, E., and Lippincott-Schwartz, J. (2008). High-density mapping of single-molecule trajectories with photoactivated localization microscopy. Nat Methods *5*, 155.

22. Rossier, O., and Giannone, G. (2016). The journey of integrins and partners in a complex interactions landscape studied by super-resolution microscopy and single protein tracking. Exp. Cell Res. *343*, 28–34.

23. Kanchanawong, P., Shtengel, G., Pasapera, A.M., Ramko, E.B., Davidson, M.W., Hess, H.F., and Waterman, C.M. (2010). Nanoscale architecture of integrin-based cell adhesions. Nature *468*, 580–584.

24. Rossier, O., Octeau, V., Sibarita, J.-B.B., Leduc, C., Tessier, B., Nair, D., Gatterdam, V., Destaing, O., Albiges-Rizo, C., Tampe, R., *et al.* (2012). Integrins beta1 and beta3 exhibit distinct dynamic nanoscale organizations inside focal adhesions. Nat Cell Biol *14*, 1057–1067.

25. Xu, K., Zhong, G., and Zhuang, X. (2013). Actin, spectrin, and associated proteins form a periodic cytoskeletal structure in axons. Science *339*, 452–6.

26. Chazeau, A., Mehidi, A., Nair, D., Gautier, J.J., Leduc, C., Chamma, I., Kage, F., Kechkar, A., Thoumine, O., Rottner, K., *et al.* (2014). Nanoscale segregation of actin nucleation and elongation factors determines dendritic spine protrusion. EMBO J. *33*, 2745–64.

27. Rottner, K., Behrendt, B., Small, J.V., and Wehland, J. (1999). VASP dynamics during lamellipodia protrusion. Nat Cell Biol *1*, 321–322.

28. Suetsugu, S., Yamazaki, D., Kurisu, S., and Takenawa, T. (2003). Differential roles of WAVE1 and WAVE2 in dorsal and peripheral ruffle formation for fibroblast cell migration. Dev Cell *5*, 595–609.

29. Machacek, M., Hodgson, L., Welch, C., Elliott, H., Pertz, O., Nalbant, P., Abell, A., Johnson, G.L., Hahn, K.M., and Danuser, G. (2009). Coordination of Rho GTPase activities during cell protrusion. Nature *461*, 99–103.

30. Pertz, O., Hodgson, L., Klemke, R.L., and Hahn, K.M. (2006). Spatiotemporal dynamics of RhoA activity in migrating cells. Nature *440*, 1069–1072.

31. Lebensohn, A.M., and Kirschner, M.W. (2009). Activation of the WAVE complex by coincident signals controls actin assembly. Mol. Cell *36*, 512–24.

32. Innocenti, M., Zucconi, A., Disanza, A., Frittoli, E., Areces, L.B., Steffen, A., Stradal, T.E.B., Di Fiore, P.P., Carlier, M.-F.F., and Scita, G. (2004). Abi1 is essential for the formation and activation of a WAVE2 signalling complex. Nat Cell Biol *6*, 319–327.

33. Steffen, A., Rottner, K., Ehinger, J., Innocenti, M., Scita, G., Wehland, J., and Stradal, T.E.B.

(2004). Sra-1 and Nap1 link Rac to actin assembly driving lamellipodia formation. EMBO J. *23*, 749–759.

34. Orré, T., Mehidi, A., Massou, S., Rossier, O., and Giannone, G. (2018). Using single-protein tracking to study cell migration.

35. Kiosses, W.B., Shattil, S.J., Pampori, N., and Schwartz, M.A. (2001). Rac recruits high-affinity integrin alphavbeta3 to lamellipodia in endothelial cell migration. Nat Cell Biol *3*, 316–320.

36. Del Pozo, M.A., Kiosses, W.B., Alderson, N.B., Meller, N., Hahn, K.M., and Schwartz, M.A. (2002). Integrins regulate GTP-Rac localized effector interactions through dissociation of Rho-GDI. Nat Cell Biol *4*, 232–239.

37. Eden, S., Rohatgi, R., Podtelejnikov, A. V, Mann, M., and Kirschner, M.W. (2002). Mechanism of regulation of WAVE1-induced actin nucleation by Rac1 and Nck. Nature *418*, 790–793.

38. Gautreau, A., Ho, H.Y.H.Y., Li, J., Steen, H., Gygi, S.P., and Kirschner, M.W. (2004). Purification and architecture of the ubiquitous Wave complex. Proc Natl Acad Sci U S A *101*, 4379–4383.

39. Millius, A., Watanabe, N., and Weiner, O.D. (2012). Diffusion, capture and recycling of SCAR/WAVE and Arp2/3 complexes observed in cells by single-molecule imaging. J. Cell Sci. *125*, 1165–76.

40. Scita, G., Confalonieri, S., Lappalainen, P., and Suetsugu, S. (2008). IRSp53: crossing the road of membrane and actin dynamics in the formation of membrane protrusions. Trends Cell Biol. *18*, 52–60.

41. Connolly, B.A., Rice, J., Feig, L.A., and Buchsbaum, R.J. (2005). Tiam1-IRSp53 Complex Formation Directs Specificity of Rac-Mediated Actin Cytoskeleton Regulation. Mol. Cell. Biol. *25*, 4602–4614.

42. Nakagawa, H., Miki, H., Nozumi, M., Takenawa, T., Miyamoto, S., Wehland, J., and Small, J.V. (2003). IRSp53 is colocalised with WAVE2 at the tips of protruding lamellipodia and filopodia independently of Mena. J. Cell Sci. *116*, 2577–83.

43. Suetsugu, S., Kurisu, S., Oikawa, T., Yamazaki, D., Oda, A., and Takenawa, T. (2006). Optimization of WAVE2 complex-induced actin polymerization by membrane-bound IRSp53, PIP(3), and Rac. J Cell Biol *173*, 571–585.

44. Schaks, M., Singh, S.P., Kage, F., Thomason, P., Klünemann, T., Steffen, A., Blankenfeldt, W., Stradal, T.E., Insall, R.H., and Rottner, K. (2018). Distinct Interaction Sites of Rac GTPase with WAVE Regulatory Complex Have Non-redundant Functions in Vivo. Curr. Biol. *28*, 3674-3684.e6.

45. Shibata, A.C.E., Chen, L.H., Nagai, R., Ishidate, F., Chadda, R., Miwa, Y., Naruse, K., Shirai, Y.M., Fujiwara, T.K., and Kusumi, A. (2013). Rac1 recruitment to the archipelago structure of the focal adhesion through the fluid membrane as revealed by single-molecule analysis. Cytoskeleton (Hoboken). *177*, 161–177.

46. Remorino, A., De Beco, S., Cayrac, F., Di Federico, F., Cornilleau, G., Gautreau, A., Parrini, M.C., Masson, J.B., Dahan, M., and Coppey, M. (2017). Gradients of Rac1 Nanoclusters Support Spatial Patterns of Rac1 Signaling. Cell Rep. *21*, 1922–1935.

47. Davis, M.J., Ha, B.H., Holman, E.C., Halaban, R., Schlessinger, J., and Boggon, T.J. (2013). RAC1P29S is a spontaneously activating cancer-associated GTPase. Proc. Natl. Acad. Sci. *110*, 912–917.

48. Lamarche, N., Tapon, N., Stowers, L., Burbelo, P.D., Aspenström, P., Bridges, T., Chant, J., and Hall, A. (1996). Rac and Cdc42 induce actin polymerization and G1 cell cycle progression independently of p65(PAK) and the JNK/SAPK MAP kinase cascade. Cell *87*, 519–529.

49. Westwick, J.K., Lambert, Q.T., Clark, G.J., Symons, M., Van Aelst, L., Pestell, R.G., and Der, C.J. (1997). Rac regulation of transformation, gene expression, and actin organization by multiple, PAK-independent pathways. Mol. Cell. Biol. *17*, 1324–35.

50. García-Mata, R., Wennerberg, K., Arthur, W.T., Noren, N.K., Ellerbroek, S.M., and Burridge, K. (2006). Analysis of activated GAPs and GEFs in cell lysates. Methods Enzymol. *406*, 425–437.

51. Pertz, O. (2010). Spatio-temporal Rho GTPase signaling - where are we now? J. Cell Sci. *123*, 1841–1850.

52. Cherfils, J., and Zeghouf, M. (2013). Regulation of Small GTPases by GEFs, GAPs, and GDIs. Physiol. Rev. *93*, 269–309.

53. Huang, F., Hartwich, T.M.P., Rivera-Molina, F.E., Lin, Y., Duim, W.C., Long, J.J., Uchil, P.D., Myers, J.R., Baird, M.A., Mothes, W., *et al.* (2013). Video-rate nanoscopy using sCMOS camera-specific single-molecule localization algorithms. Nat. Methods *10*, 653–658.

54. Valon, L., Etoc, F., Remorino, A., Di Pietro, F., Morin, X., Dahan, M., and Coppey, M. (2015). Predictive Spatiotemporal Manipulation of Signaling Perturbations Using Optogenetics. Biophys. J. *109*, 1785–1797.

55. Martin, K., Reimann, A., Fritz, R.D., Ryu, H., Jeon, N.L., and Pertz, O. (2016). Spatio-temporal co-ordination of RhoA, Rac1 and Cdc42 activation during prototypical edge protrusion and retraction dynamics. Sci. Rep. *6*, 21901.

56. Wolfenson, H., Meacci, G., Liu, S., Stachowiak, M.R., Iskratsch, T., Ghassemi, S., Roca-Cusachs, P., O'Shaughnessy, B., Hone, J., and Sheetz, M.P. (2016). Tropomyosin controls sarcomere-like contractions for rigidity sensing and suppressing growth on soft matrices. Nat. Cell Biol. *18*, 33–42.

57. Tkachenko, E., Sabouri-Ghomi, M., Pertz, O., Kim, C., Gutierrez, E., Machacek, M., Groisman, A., Danuser, G., and Ginsberg, M.H. (2011). Protein kinase A governs a RhoA-RhoGDI protrusion-retraction pacemaker in migrating cells. Nat Cell Biol *13*, 660–667.

58. Isogai, T., van der Kammen, R., Leyton-Puig, D., Kedziora, K.M., Jalink, K., and Innocenti, M. (2015). Initiation of lamellipodia and ruffles involves cooperation between mDia1 and the Arp2/3 complex. J. Cell Sci. *128*, 3796–3810.

59. Paszek, M.J., DuFort, C.C., Rossier, O., Bainer, R., Mouw, J.K., Godula, K., Hudak, J.E., Lakins, J.N., Wijekoon, A.C., Cassereau, L., *et al.* (2014). The cancer glycocalyx mechanically primes integrin-mediated growth and survival. Nature *511*, 319–325.

60. Galbraith, C.G., Yamada, K.M., and Galbraith, J.A. (2007). Polymerizing actin fibers position integrins primed to probe for adhesion sites. Science (80-.). *315*, 992–995.

61. del Pozo, M.A., Price, L.S., Alderson, N.B., Ren, X.D., and Schwartz, M.A. (2000). Adhesion to the extracellular matrix regulates the coupling of the small GTPase Rac to its effector PAK. EMBO J *19*, 2008–2014.

62. Wang, S., Watanabe, T., Matsuzawa, K., Katsumi, A., Kakeno, M., Matsui, T., Ye, F., Sato, K., Murase, K., Sugiyama, I., *et al.* (2012). Tiam1 interaction with the PAR complex promotes talin-mediated Rac1 activation during polarized cell migration. J. Cell Biol. *199*, 331–345.

63. Kuo, J.C., Han, X., Hsiao, C.T., Yates 3rd, J.R., and Waterman, C.M. (2011). Analysis of the myosin-II-responsive focal adhesion proteome reveals a role for beta-Pix in negative regulation of focal adhesion maturation. Nat Cell Biol *13*, 383–393.

64. Law, A.L., Vehlow, A., Kotini, M., Dodgson, L., Soong, D., Theveneau, E., Bodo, C., Taylor, E., Navarro, C., Perera, U., *et al.* (2013). Lamellipodin and the Scar/WAVE complex cooperate to promote cell migration in vivo. J. Cell Biol. *203*, 673–689.

65. Chen, X.J.J., Squarr, A.J.J., Stephan, R., Chen, B., Higgins, T.E.E., Barry, D.J.J., Martin, M.C.C., Rosen, M.K.K., Bogdan, S., and Way, M. (2014). Ena/VASP Proteins Cooperate with the WAVE Complex to Regulate the Actin Cytoskeleton. Dev. Cell *30*, 569–84.

66. Das, S., Yin, T., Yang, Q., Zhang, J., Wu, Y.I., and Yu, J. (2015). Single-molecule tracking of small GTPase Rac1 uncovers spatial regulation of membrane translocation and mechanism for polarized signaling. Proc. Natl. Acad. Sci. U. S. A.

67. Blanchoin, L., Amann, K.J., Higgs, H.N., Marchand, J.B., Kaiser, D.A., and Pollard, T.D. (2000). Direct observation of dendritic actin filament networks nucleated by Arp2/3 complex and WASP/Scar proteins. Nature *404*, 1007–1011.

68. Lee, K., Gallop, J.L., Rambani, K., and Kirschner, M.W. (2010). Self-assembly of filopodia-like structures on supported lipid bilayers. Science *329*, 1341–5.

69. Reymann, A.-C., Boujemaa-Paterski, R., Martiel, J.-L., Guérin, C., Cao, W., Chin, H.F., De La Cruz, E.M., Théry, M., and Blanchoin, L. (2012). Actin network architecture can determine myosin motor activity. Science *336*, 1310–4.

70. Su, J., Muranjan, M., and Sap, J. (1999). Receptor protein tyrosine phosphatase α activates Src-family kinases and controls integrin-mediated responses in fibroblasts. Curr. Biol. *9*, 505–511.

71. Izeddin, I., Boulanger, J., Racine, V., Specht, C.G., Kechkar, A., Nair, D., Triller, A., Choquet, D., Dahan, M., and Sibarita, J.B. (2012). Wavelet analysis for single molecule localization microscopy. Opt Express *20*, 2081–2095.

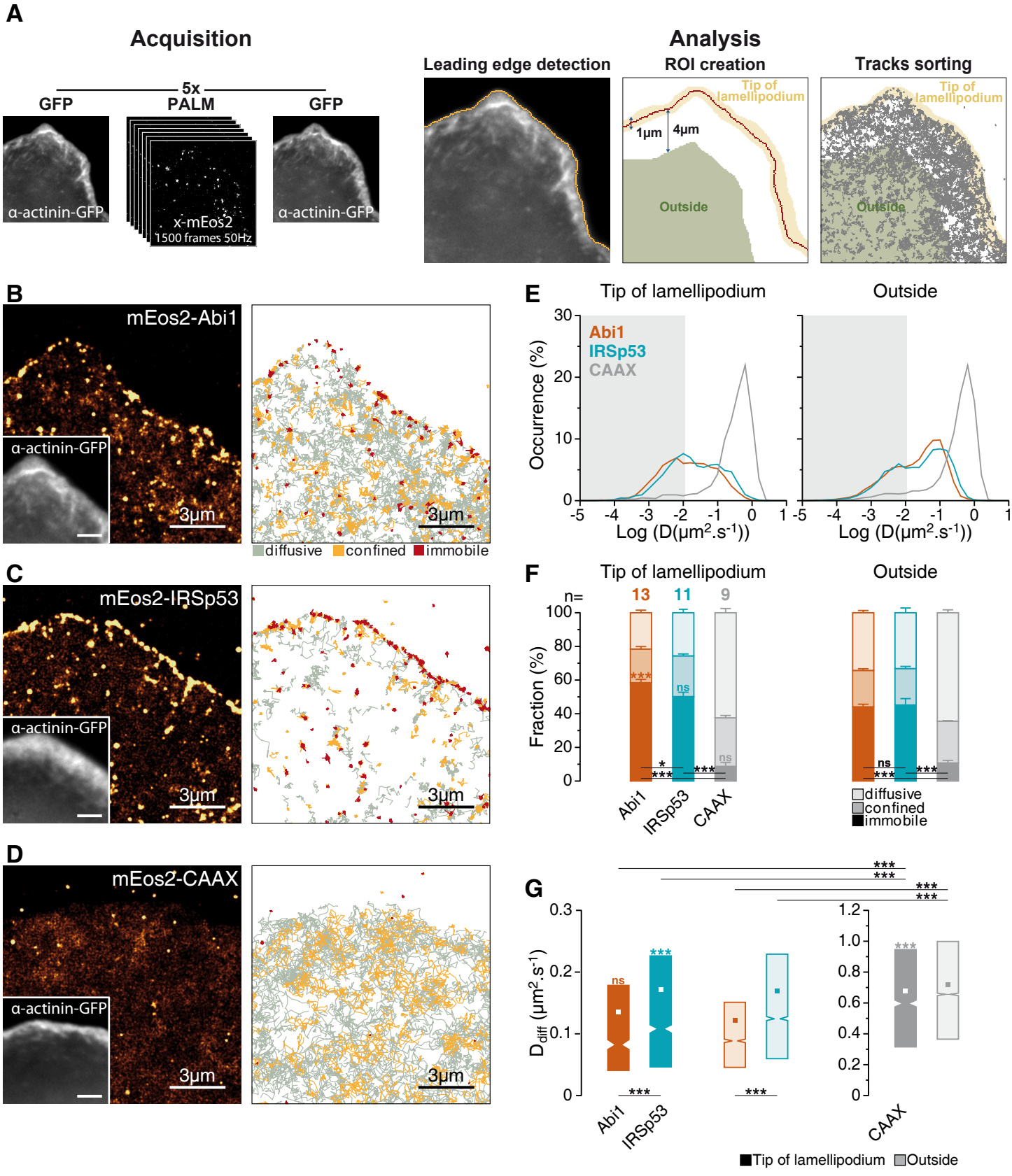
A
Acquisition
5x
GFP
PALM
GFP
α-actinin-GFP
x-mEos2
1500 frames 50Hz
α-actinin-GFP
Analysis
Leading edge detection
ROI creation
Tracks sorting
Tip of lamellipodium
1µm
4µm
Outside
Tip of lamellipodium
Outside
B
mEos2-Abi1
α-actinin-GFP
3µm
3µm
diffusive
confined
immobile
C
mEos2-IRSp53
α-actinin-GFP
3µm
3µm
D
mEos2-CAAX
α-actinin-GFP
3µm
3µm
E
Tip of lamellipodium
Outside
Abi1
IRSp53
CAAX
Occurrence (%)
Log (D(µm².s⁻¹))
Log (D(µm².s⁻¹))
F
Tip of lamellipodium
Outside
n=
13
11
9
Fraction (%)
Abi1
IRSp53
CAAX
diffusive
confined
immobile
G
D_diff (µm².s⁻¹)
Abi1
IRSp53
CAAX
Tip of lamellipodium
Outside

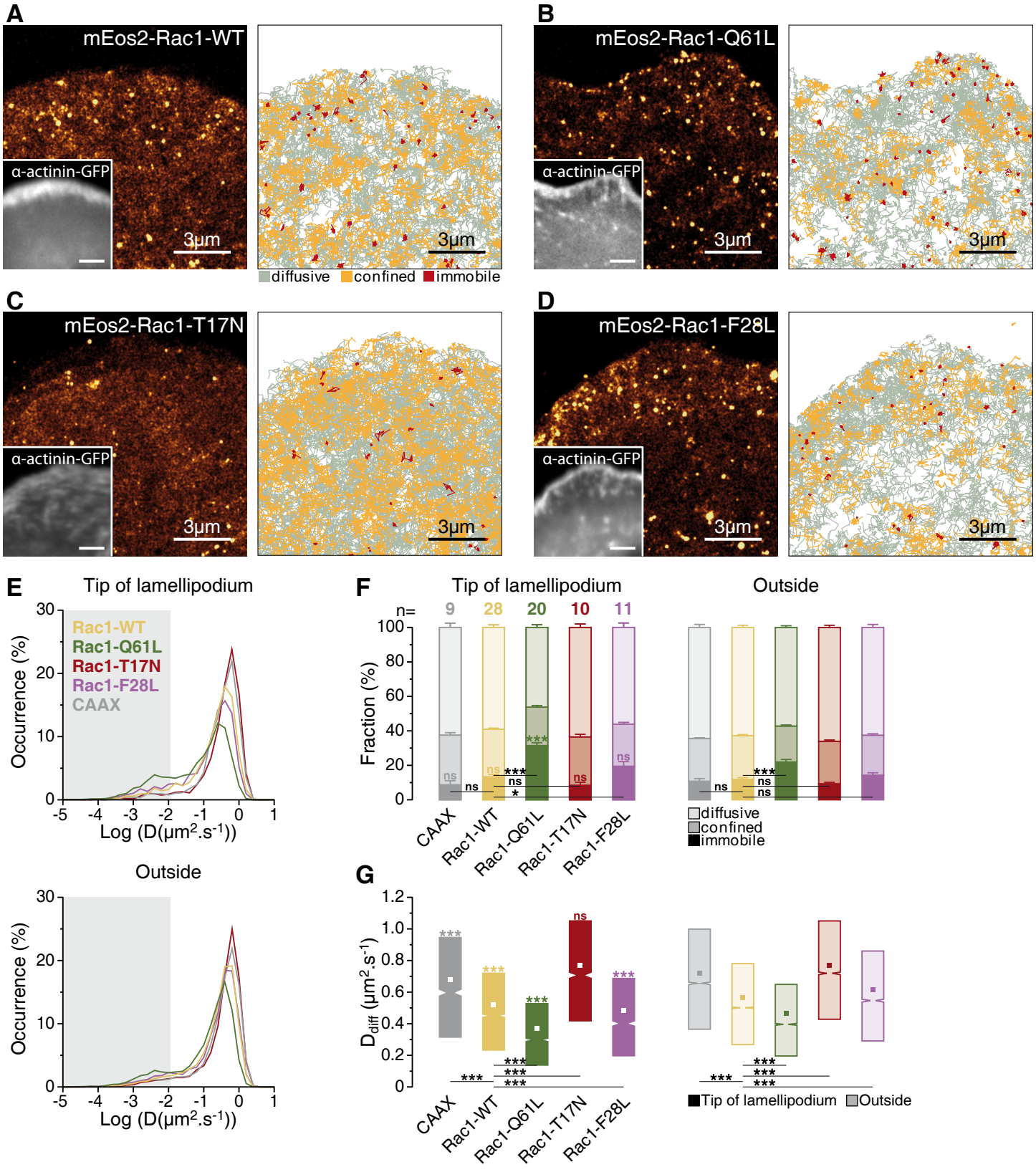
A
mEos2-Rac1-WT
α-actinin-GFP
3µm
3µm
diffusive
confined
immobile
B
mEos2-Rac1-Q61L
α-actinin-GFP
3µm
3µm
C
mEos2-Rac1-T17N
α-actinin-GFP
3µm
3µm
D
mEos2-Rac1-F28L
α-actinin-GFP
3µm
3µm
E
Tip of lamellipodium
Rac1-WT
Rac1-Q61L
Rac1-T17N
Rac1-F28L
CAAX
Occurrence (%)
Log (D(µm².s⁻¹))
Outside
Occurrence (%)
Log (D(µm².s⁻¹))
F
Tip of lamellipodium
Outside
n=
9
28
20
10
11
Fraction (%)
CAAX
Rac1-WT
Rac1-Q61L
Rac1-T17N
Rac1-F28L
diffusive
confined
immobile
G
D_diff (µm².s⁻¹)
CAAX
Rac1-WT
Rac1-Q61L
Rac1-T17N
Rac1-F28L
Tip of lamellipodium
Outside

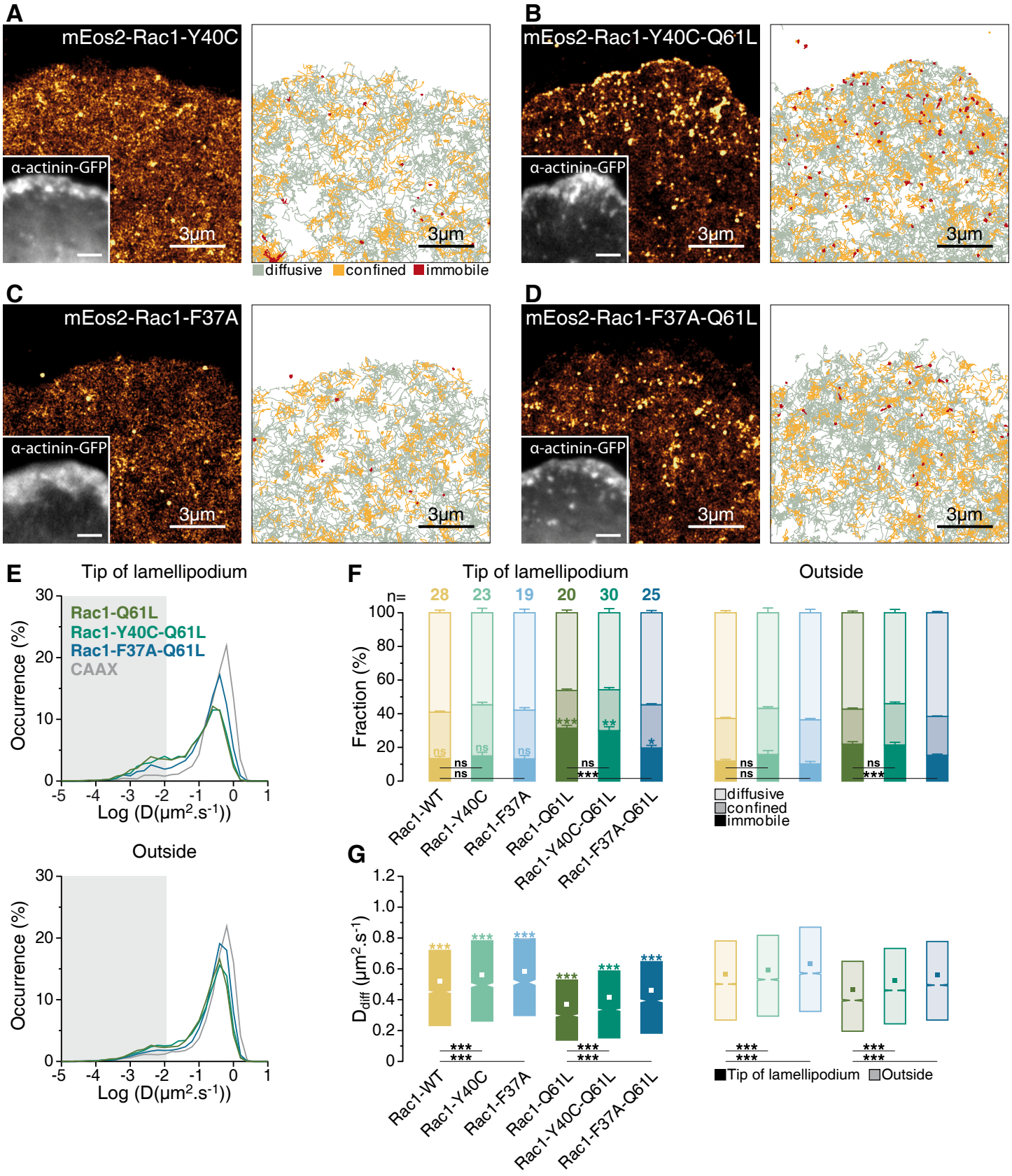
A
mEos2-Rac1-Y40C
α-actinin-GFP
3µm
3µm
diffusive
confined
immobile
B
mEos2-Rac1-Y40C-Q61L
α-actinin-GFP
3µm
3µm
C
mEos2-Rac1-F37A
α-actinin-GFP
3µm
3µm
D
mEos2-Rac1-F37A-Q61L
α-actinin-GFP
3µm
3µm
E
Tip of lamellipodium
Rac1-Q61L
Rac1-Y40C-Q61L
Rac1-F37A-Q61L
CAAX
Occurrence (%)
Log (D(µm².s⁻¹))
Outside
Occurrence (%)
Log (D(µm².s⁻¹))
F
Tip of lamellipodium
Outside
n=
28
23
19
20
30
25
Fraction (%)
Rac1-WT
Rac1-Y40C
Rac1-F37A
Rac1-Q61L
Rac1-Y40C-Q61L
Rac1-F37A-Q61L
diffusive
confined
immobile
G
D_diff (µm².s⁻¹)
Tip of lamellipodium
Outside

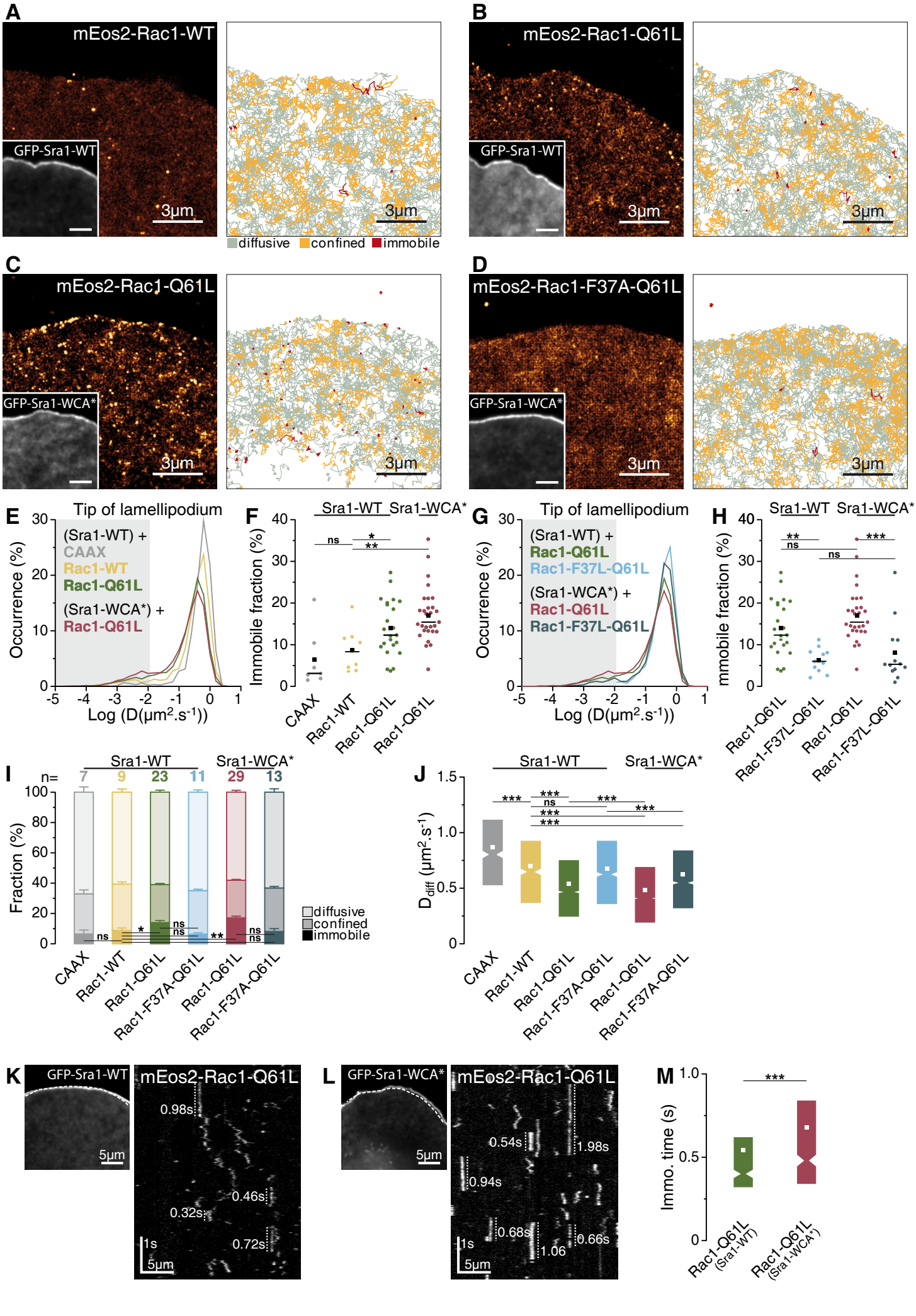
A
mEos2-Rac1-WT
GFP-Sra1-WT
3µm
3µm
diffusive confined immobile
B
mEos2-Rac1-Q61L
GFP-Sra1-WT
3µm
3µm
C
mEos2-Rac1-Q61L
GFP-Sra1-WCA*
3µm
3µm
D
mEos2-Rac1-F37A-Q61L
GFP-Sra1-WCA*
3µm
3µm
E
Tip of lamellipodium
(Sra1-WT) +
CAAX
Rac1-WT
Rac1-Q61L
(Sra1-WCA*) +
Rac1-Q61L
Occurrence (%)
Log (D(µm².s⁻¹))
F
Sra1-WT Sra1-WCA*
Immobile fraction (%)
ns
*
**
CAAX
Rac1-WT
Rac1-Q61L
Rac1-Q61L
G
Tip of lamellipodium
(Sra1-WT) +
Rac1-Q61L
Rac1-F37L-Q61L
(Sra1-WCA*) +
Rac1-Q61L
Rac1-F37L-Q61L
Occurrence (%)
Log (D(µm².s⁻¹))
H
Sra1-WT Sra1-WCA*
mmobile fraction (%)
**
ns
ns
***
Rac1-Q61L
Rac1-F37L-Q61L
Rac1-Q61L
Rac1-F37L-Q61L
I
Sra1-WT
Sra1-WCA*
n= 7 9 23 11 29 13
Fraction (%)
ns
*
ns
ns
**
ns
ns
diffusive
confined
immobile
CAAX
Rac1-WT
Rac1-Q61L
Rac1-F37A-Q61L
Rac1-Q61L
Rac1-F37A-Q61L
J
Sra1-WT
Sra1-WCA*
D_diff (µm².s⁻¹)
***
***
ns
***
***
***
***
CAAX
Rac1-WT
Rac1-Q61L
Rac1-F37A-Q61L
Rac1-Q61L
Rac1-F37A-Q61L
K
GFP-Sra1-WT
5µm
mEos2-Rac1-Q61L
0.98s
0.46s
0.32s
0.72s
1s
5µm
L
GFP-Sra1-WCA*
5µm
mEos2-Rac1-Q61L
0.54s
1.98s
0.94s
0.68s
0.66s
1.06
1s
5µm
M
Immo. time (s)
***
Rac1-Q61L (Sra1-WT)
Rac1-Q61L (Sra1-WCA*)

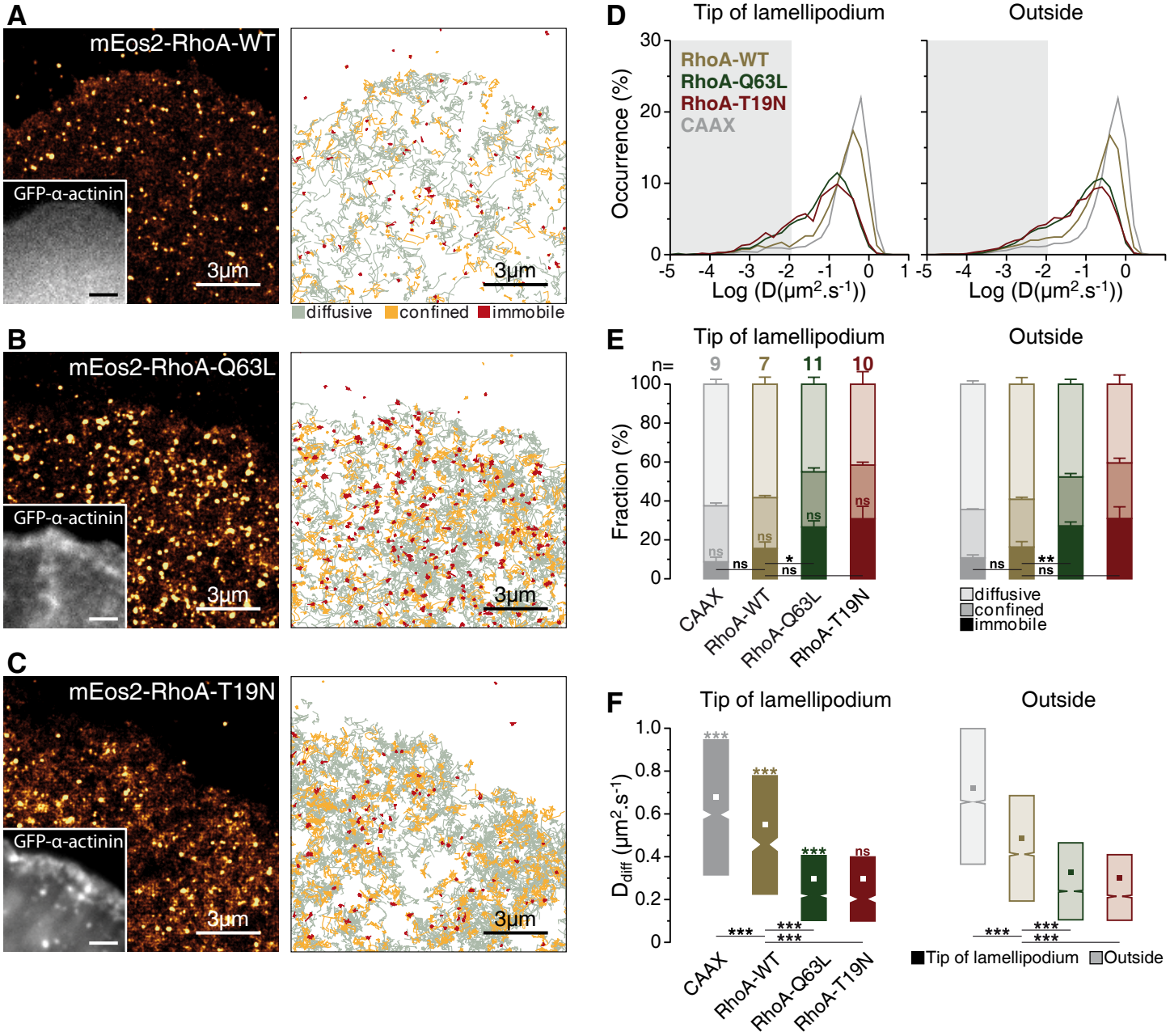
A
mEos2-RhoA-WT
GFP-α-actinin
3µm
3µm
diffusive
confined
immobile
B
mEos2-RhoA-Q63L
GFP-α-actinin
3µm
3µm
C
mEos2-RhoA-T19N
GFP-α-actinin
3µm
3µm
D
Tip of lamellipodium
Outside
RhoA-WT
RhoA-Q63L
RhoA-T19N
CAAX
Occurrence (%)
Log (D(µm².s⁻¹))
Log (D(µm².s⁻¹))
E
Tip of lamellipodium
Outside
n=
9
7
11
10
Fraction (%)
CAAX
RhoA-WT
RhoA-Q63L
RhoA-T19N
diffusive
confined
immobile
F
Tip of lamellipodium
Outside
D_diff (µm².s⁻¹)
CAAX
RhoA-WT
RhoA-Q63L
RhoA-T19N
Tip of lamellipodium
Outside

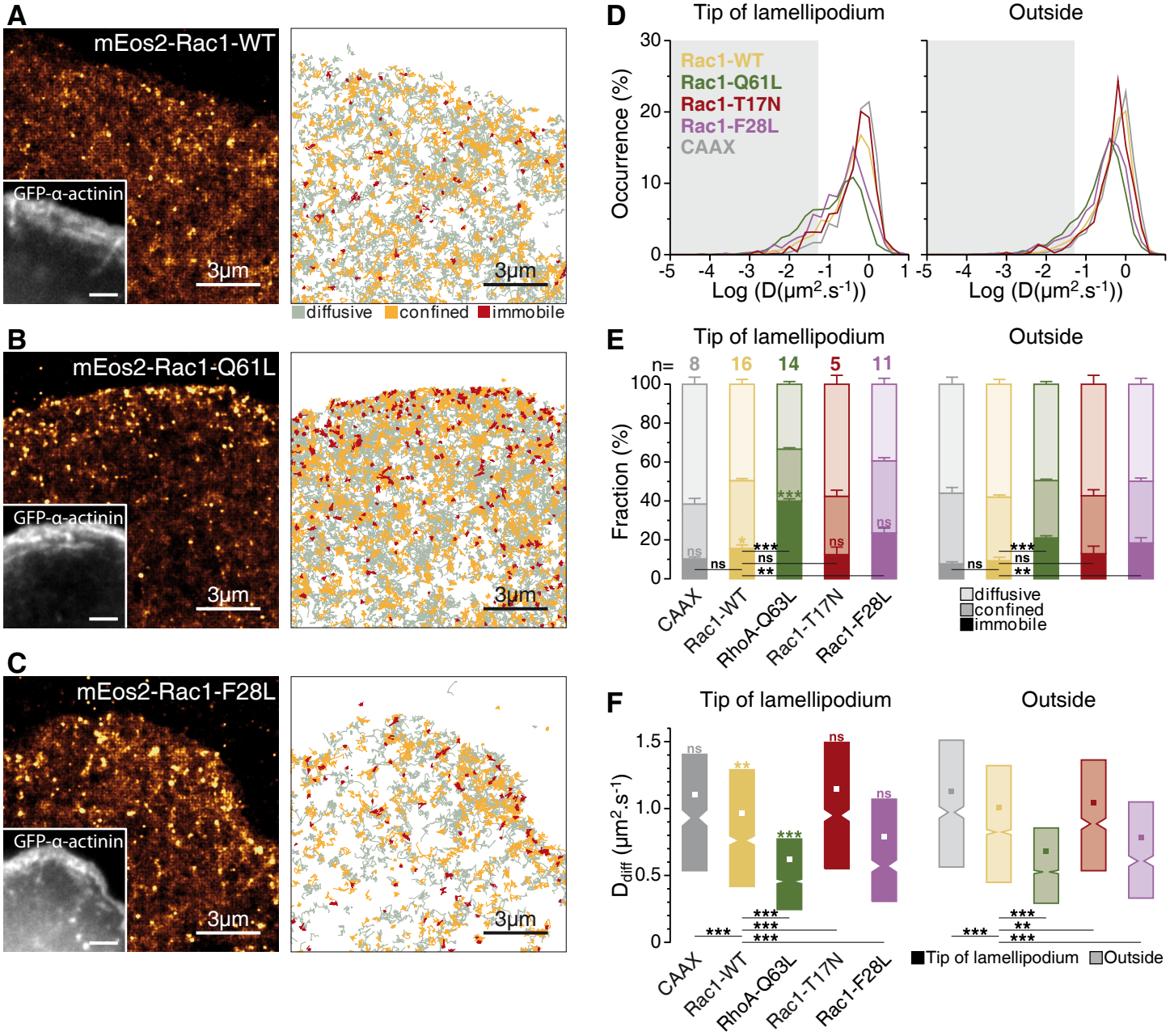
A
mEos2-Rac1-WT
GFP-α-actinin
3µm
3µm
diffusive
confined
immobile
B
mEos2-Rac1-Q61L
GFP-α-actinin
3µm
3µm
C
mEos2-Rac1-F28L
GFP-α-actinin
3µm
3µm
D
Tip of lamellipodium
Outside
Rac1-WT
Rac1-Q61L
Rac1-T17N
Rac1-F28L
CAAX
Occurrence (%)
Log (D(µm².s⁻¹))
E
Tip of lamellipodium
Outside
n= 8 16 14 5 11
Fraction (%)
CAAX
Rac1-WT
RhoA-Q63L
Rac1-T17N
Rac1-F28L
diffusive
confined
immobile
F
Tip of lamellipodium
Outside
D_diff (µm².s⁻¹)
Tip of lamellipodium
Outside

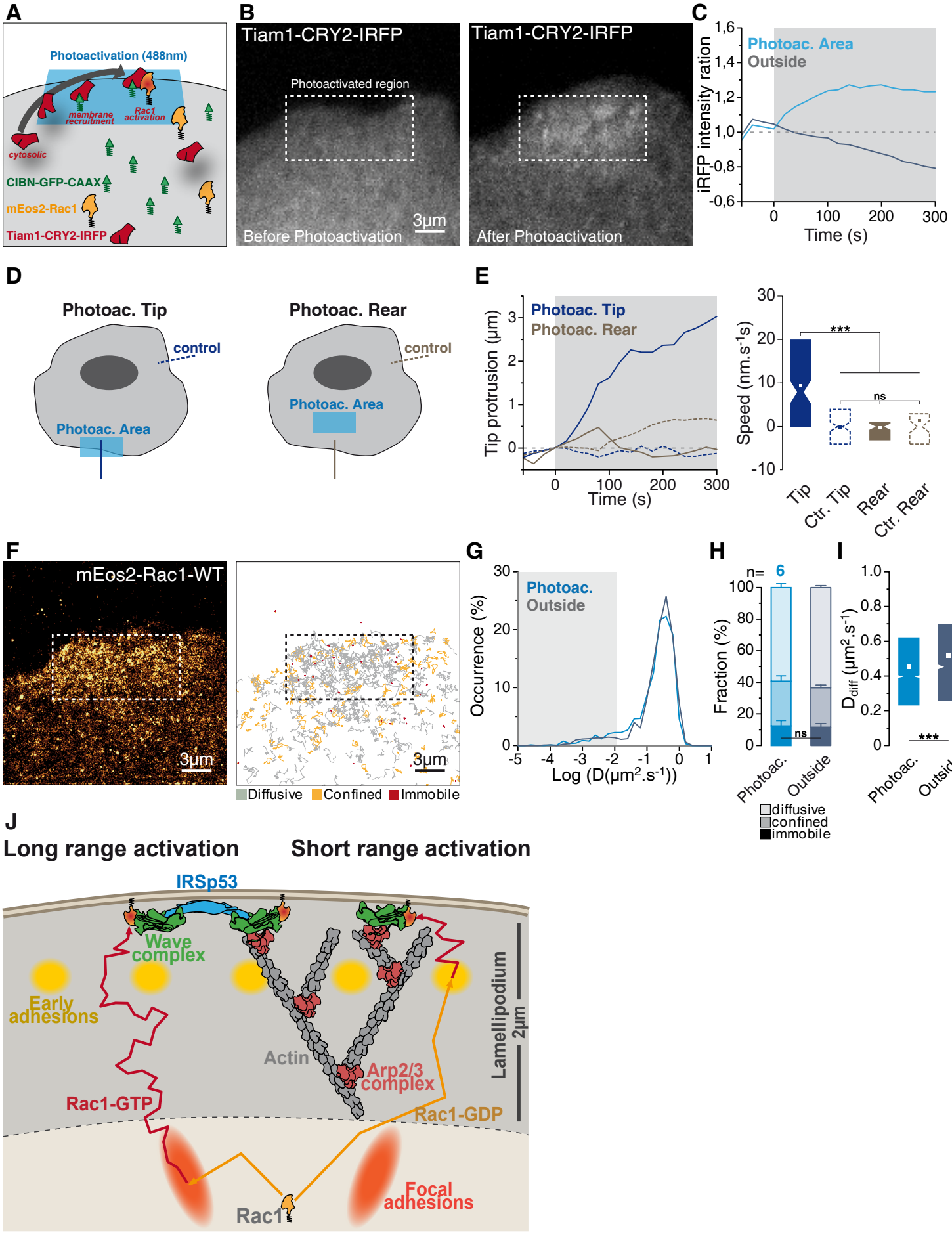
A
Photoactivation (488nm)
membrane recruitment
Rac1 activation
cytosolic
CIBN-GFP-CAAX
mEos2-Rac1
Tiam1-CRY2-IRFP
B
Tiam1-CRY2-IRFP
Photoactivated region
Before Photoactivation
3µm
Tiam1-CRY2-IRFP
After Photoactivation
C
Photoac. Area
Outside
iRFP intensity ration
Time (s)
D
Photoac. Tip
control
Photoac. Area
Photoac. Rear
control
Photoac. Area
E
Photoac. Tip
Photoac. Rear
Tip protrusion (µm)
Time (s)
Speed (nm.s-1s)
***
ns
Tip
Ctr. Tip
Rear
Ctr. Rear
F
mEos2-Rac1-WT
3µm
3µm
Diffusive
Confined
Immobile
G
Photoac.
Outside
Occurrence (%)
Log (D(µm2.s-1))
H
n= 6
Fraction (%)
ns
Photoac.
Outside
diffusive
confined
immobile
I
Ddiff (µm2.s-1)
***
Photoac.
Outside
J
Long range activation
Short range activation
IRSp53
Wave complex
Early adhesions
Actin
Arp2/3 complex
Lamellipodium
2µm
Rac1-GTP
Rac1-GDP
Focal adhesions
Rac1

Single Protein Tracking

Local optogenetic activation

Transient immobilization of activated Rac1

Tip

Lamellipodium

Rear

Rac1 membrane free-diffusion

Rac1 photoactivation

Membrane protrusions

Rac1 photoactivation

No membrane protrusions

Membrane protrusions

Local fast cycles of activation /inactivation

Inactive Rac1

GDP

Active Rac1

GTP

WAVE Regulatory Complex (WRC)

Arp2/3 Complex

Actin

Membrane free-diffusion

GDP

Active Rac1

Sra1

Rac1 immobilization at the tip depends on WRC binding